# Genetic mutations linked to Parkinson's disease differentially control nucleolar activity in pre-symptomatic mouse models.

V. Evsyukov[1,9], A. Domanskyi[2,3,9], H. Bierhoff[4,5,6], S. Gispert[7], R. Mustafa[1,8], F. Schlaudraff[8], B. Liss[8], R. Parlato[1,8*].

[1] Institute of Anatomy and Medical Cell Biology, University of Heidelberg, Heidelberg, Germany

[2] German Cancer Research Center, Molecular Biology of the Cell I, Heidelberg, Germany

[3] Institute of Biotechnology, University of Helsinki, Helsinki, Finland

[4] German Cancer Research Center, Molecular Biology of the Cell II, Heidelberg, Germany

[5] Department of Biochemistry, Institute of Biochemistry and Biophysics, Center for Molecular Biomedicine (CMB), Friedrich Schiller University Jena, Germany

[6] Leibniz-Institute on Aging – Fritz Lipmann Institute (FLI), Jena, Germany

[7] Experimental Neurology, Goethe University Medical School, Frankfurt am Main, Germany

[8] Institute of Applied Physiology, University of Ulm, Ulm, Germany

[9] Equal contribution

*** Corresponding Author**

Dr. Rosanna Parlato

Institute of Applied Physiology

University of Ulm

Albert Einstein Allee 11, 89081 Ulm, Germany.

E-mail: rosanna.parlato@uni-ulm.de.

Phone: +49-731-500-36214; FAX: +49-731-500-36202.



Disease Models & Mechanisms • DMM • Advance article

## SUMMARY STATEMENT

This study shows that genetic mutations linked to Parkinson's disease lead to stage-specific deregulation of the nucleolus, a major integrator of the cellular stress response.


## ABSTRACT

Genetic mutations underlying neurodegenerative disorders impair ribosomal DNA (rDNA) transcription suggesting nucleolar dysfunction as a novel pathomechanism in polyglutamine diseases and in certain forms of amyotrophic lateral sclerosis/frontotemporal dementia. Here, we investigated nucleolar activity in pre-symptomatic digenic models of Parkinson's disease (PD) modeling the multifactorial etiology of this disease.

To this end, we analyzed a novel mouse model mildly overexpressing the mutant human-A53T-alpha-synuclein (hA53T-SNCA/PARK1) in a PTEN-induced kinase 1 (PINK1/PARK6) knock-out background and mutant mice lacking both DJ-1/PARK7 and PINK1/PARK6. We showed that overexpressed human-A53T-alpha-synuclein localizes in the nucleolus. Moreover, these mutants show a progressive reduction of rDNA transcription linked to a reduced mouse lifespan. On the contrary in DJ-1/PINK1 double knock-out (DKO) mice rDNA transcription is preserved. mRNA levels of the nucleolar transcription initiation factor-IA (TIF-IA) decrease in substantia nigra of PD patients. Because loss of TIF-IA, as a tool to mimic nucleolar stress, increases oxidative stress and because DJ-1 and PINK1 mutations result in higher vulnerability to oxidative stress, we further explored the synergism between these PD-associated genes and impaired nucleolar function. By the conditional ablation of TIF-IA gene, we blocked ribosomal RNA (rRNA) synthesis in adult dopaminergic neurons in a DJ-1/PINK1 DKO background. However, the early phenotype of these triple knock-out mice was similar to those mice exclusively lacking TIF-IA. These data sustain a model in which DJ-1/PINK1 loss does not impair nucleolar activity in a pre-symptomatic stage. This is the first study that analyzes nucleolar function in digenic PD models. We can conclude that at least in these models the nucleolus is not as severely disrupted as previously shown in DA neurons from PD patients and neurotoxin-based PD mouse models. The results also show that early increase in rDNA transcription and nucleolar integrity may represent specific homeostatic responses in these digenic pre-symptomatic PD models.



**Key words: Nucleolus, Parkinson's disease, neuronal homeostasis**

## INTRODUCTION

The nucleolus is an emerging controller of neuronal homeostasis and a central regulator of the cellular stress response (Boulon et al., 2010). Nucleolar activity is tightly linked to the cellular well-being as rRNA synthesis decreases in response to adverse extracellular conditions including DNA damage, oxidative stress, and neurotrophic withdrawal (Hetman and Pietrzak, 2012). Accordingly, reduced rDNA transcription and disruption of nucleolar integrity are common to several neurodegenerative disorders (Grummt, 2013, Parlato and Kreiner, 2013). Interestingly, mutant proteins and RNAs may directly interfere with the RNA polymerase I machinery reducing the level of rDNA transcription in polyglutamine diseases, including Huntington's disease (HD) and in some forms of amyotrophic lateral sclerosis and fronto-temporal dementia (ALS/FTD) (Parlato and Bierhoff, 2015).

Impaired nucleolar activity and disrupted nucleolar integrity, known as nucleolar stress, have also been reported in Parkinson's disease (PD) autopsies in dopaminergic (DA) neurons (Rieker et al., 2011, Parlato and Liss, 2014). Notably nucleolar stress is evident in neurotoxin-based PD mouse models by the analysis of rDNA synthesis and altered distribution of nucleolar proteins (Rieker et al., 2011, Healy-Stoffel et al., 2013). We have previously shown that induction of nucleolar stress in DA neurons leads to progressive and selective degeneration of substantia nigra (SN), impaired mitochondrial function and increased oxidative stress linked to downregulation of the mammalian target of rapamycin (mTOR) pathway (Rieker et al., 2011, Kreiner et al., 2013). The observation that neuronal death is accelerated in the acute neurotoxin-based *N*-methyl-4-phenyl-1,2,3,6-tetrahydropyridine (MPTP) model upon nucleolar stress revealed a mechanistic crosstalk between impaired nucleoli and mitochondria (Rieker et al., 2011).

Most of PD cases are idiopathic, about 10% of PD cases are Mendelian-inherited and about 27% of heritability has been recently estimated (Mullin and Schapira, 2015). Several genetic mutations and risk factors for PD have been identified, revealing shared and converging pathophysiological pathways (Mullin and Schapira, 2015, Kumaran and Cookson, 2015, Duda et al., 2016). Interestingly, a PD-linked mutant form of the DJ-1 (PARK7) gene impaired maturation of rRNA in a cellular PD model upon proteasome inhibition (Vilotti et al., 2012). Conditional ablation of parkin (PARK2) in DA neurons results in reduced level of precursor rRNA (pre-rRNA) transcripts and release of nucleolar proteins in the nucleus, a sign of nucleolar stress (Kang and Shin, 2014).

Despite the emerging evidence, the time- and cell-specific link between genetic mutations accounting for PD and nucleolar activity is still poorly investigated. To this end, mouse models based on PD genetic mutations represent a very convenient tool to dissect mechanisms underlying neuronal homeostasis in pre-symptomatic PD stages, as in general they are not affected by neuronal death (Dawson et al., 2010). DJ-1 and PINK1 (PARK6) for example are known to protect against oxidative stress and to regulate mitochondrial function and clearance (Kim et al., 2005, Narendra et al., 2010). Mutations in these genes cause autosomal recessive early-onset PD; however compensatory mechanisms have been reported in the knock-out mice, in which DA neuronal survival is not impaired even in aged mutant mice (Pham et al., 2010, Glasl et al., 2012). This lack of DA neurodegeneration is also observed in transgenic mice overexpressing PD-related alpha-synuclein point mutations sustaining the hypothesis that PD is a multifactorial neurodegenerative disorder (Dawson et al., 2010).

To focus the analysis on the integration of multiple pathways in PD, we performed a systematic analysis of rDNA transcription and nucleolar integrity in a novel digenic mouse model of PD. In this model the heterologous prion promoter drives an exclusively neuronal overexpression (1.5-fold) of the PD-triggering human A53T point mutation in the alpha-synuclein protein (A53T-SNCA) (Gispert et al., 2003, Kurz et al., 2010). This mouse line was named hA53T-SNCA, and is also known as PrPmtA. In the double mutant mice, this mild overexpression of human mutant A53T-SNCA as a neurotoxic stressor is complemented with a PTEN-induced kinase 1 (PINK1) knock-out background leading to a loss of stress-responses (hA53T-SNCA/PINK1KO) at different stages (Gispert et al., 2015, Auburger et al., 2016). hA53T-SNCA/PINK1KO mice showed a phenotype more severe than each respective single mutant, in particular spontaneous activity at 3 months and lifespan were reduced, concomitantly with altered degradation and aggregation of alpha-synuclein at 18 months (Gispert et al., 2015). These characteristics were crucial when this mouse line was chosen for this study.

In addition, we studied adult mutant mice lacking DJ-1 and PINK1 (Pham et al., 2010, Glasl et al., 2012). DJ-1 KO mice show ca. 6% DA neuronal loss only in the ventral tegmental area independently of age and slight alterations in exploratory/motivational and cognitive behavior (Pham et al., 2010). PINK1 KO mice show alterations in gait and olfactory function, but no alterations in DA neuron survival examined at 6 and 19 months (Glasl et al., 2012). Previous studies based on the triple KO of Parkin, DJ-1 and PINK1 have also shown no effects on DA neuronal survival at least until 24 months (Kitada et al., 2009). These

combined genetic models were therefore suitable to investigate the impact of PD-related genes on nucleolar function in pre-symptomatic models independently of DA neuronal loss.

We showed that the hA53T-SNCA mutation in a PINK1 KO background leads to reduced pre-rRNA levels and changes in number of nucleoli, accompanied by the progression towards a more severe phenotype. On the contrary, DJ-1 and PINK1 double knock-out mice do not show reduced levels of rRNA synthesis. Because loss of DJ-1 and PINK1 and inhibition of rRNA synthesis alter mitochondrial function and render DA neurons more vulnerable to oxidative stress, we further investigated the functional link between these PARK genes and impaired nucleolar activity, that is known to increase oxidative stress (Rieker et al., 2011, Kreiner et al., 2013). We induced nucleolar stress in adult mice by the conditional genetic ablation of the RNA polymerase I regulator transcription initiation factor-IA (TIF-IA) in the DJ-1 and PINK1 null background (Rieker et al., 2011). The phenotype of the TIF-IA single mutants was not enhanced in the triple knock-out mice, further indicating that DJ-1/PINK1 loss does not regulate nucleolar function in these mouse models of pre-symptomatic PD.

Taken together, these results support the role of nucleolar-dependent mechanisms in the pre-symptomatic PD phase, and revealed differential effects of PARK mutations on nucleolar activity of SN DA neurons, as well as on homeostatic responses that target nucleolar function in preclinical stages.

## RESULTS

### Nucleolar activity is altered in a pre-symptomatic PD model based on mild overexpression of human A53T-alpha-synuclein in a PINK1 null genetic background.

In hA53T-SNCA/PINK1KO mice behavioral abnormalities occur at 3 months, while increased protein aggregates are visible in the ventral midbrain between 15 and 17 months (Gispert et al., 2015) and the lifespan of a subset of these mice is reduced starting from 16 months (Gispert et al., 2015). In light of these phenotypes and due to decreased viability after 16 months, we considered for our analysis 3 months-old mice as early stage, while mice comprised between 16 and 19 months represented late stages. By immunofluorescent staining with a specific human alpha-synuclein antibody we confirmed that hA53T-SNCA transgenic mice overexpress alpha-synuclein in the cytoplasm and nucleus of ventral midbrain DA neurons identified by tyrosine hydroxylase (TH) immunoreactivity at three months in comparison with wild-type (Figure 1 and Suppl. Fig.1) (Gispert et al., 2015). By the immunostaining with a nucleolin (NCL) specific antibody, to identify the nucleolus, we could show that while, as expected, hA53T-SNCA is completely absent in the wild-type DA neurons (Fig. 1A-C), this is located in the nucleus and in the nucleolus in DA neurons of hA53T-SNCA/PINK1KO mice (Figure 1D-F).

Next, to monitor rDNA transcription we detected pre-rRNA (+1/+130) and another intermediate precursor (+597/+765) by quantitative real-time PCR (qRT-PCR) in dissected ventral midbrain at 3, 16 and 18 months in hA53T-SNCA/PINK1KO and respective age-matched controls (Figure 2A-C). By this approach, the differences in pre-rRNA levels observed in hA53T-SNCA/PINK1KO mice at 18 months in concomitance with a reduced lifespan and manifestation of the symptomatic phase, were not significant (Figure 2B, C; at 18 months fold change for pre-rRNA (+1/+130): wild-type 1.00 ± 0.10, hA53T-SNCA/PINK1KO 0.69 ± 0.07, p=0.057; for pre-rRNA (+597/+765): wild-type 1.00 ± 0.13, hA53T-SNCA/PINK1KO 0.66 ± 0.06, and p=0.078 and Suppl. Fig. 2A,B). Given the heterogeneous expression of the transgene across DA neurons and the different neuron populations, to provide a deeper insight of the rate of rRNA synthesis at the level of single DA cells, we performed *in situ* hybridization (ISH) in combination with immunohistochemistry (IHC) with TH antibody and visualized full-length 47S pre-rRNA in DA neurons of SN and ventral tegmental area (VTA) in tissue sections (Figure 2A, D, E). The stained area identifying the nucleolar pre-rRNA signal was about 30% lower in hA53T-SNCA/PINK1KO mice at 19 months of age in comparison to controls, suggesting a decreased amount of 47S pre-rRNA selectively in VTA DA but not SN DA neurons of

hA53T-SNCA/PINK1KO mice (Figure 2E, right, wild-type 1.00 ± 0.01, hA53T-SNCA/PINK1KO 0.72 ± 0.06, $p<0.05$ for VTA DA neurons; wild-type 1.00 ± 0.10, hA53T-SNCA/PINK1KO 0.70 ± 0.06, $p=0.06$ for SN DA neurons and Suppl. Fig. 2C,D).

The initial description of the hA53T-SNCA transgenic mice with exclusive neuronal expression driven by the prion promoter showed human alpha-synuclein immunoreactivity also in the hippocampus (Gispert et al., 2003). Accordingly, we analyzed also in this region the area of the 47S pre-rRNA signals at late stages, however the differences between the hA53T-SNCA/PINK1KO mutant and respective control mice, were not significant (Suppl. Fig. 3, wild-type 1.00 ± 0.07, hA53T-SNCA/PINK1KO 0.85 ± 0.06, $p=0.18$).

A similar analysis performed at 3 months in DA neurons of hA53T-SNCA/PINK1KO mice did not reveal any significant changes of pre-rRNA (Figure 2E, left). Interestingly, a quantitative analysis of 47S pre-rRNA signals in DA neurons at 3 months showed that the percentage of TH positive neurons containing one nucleolus was lower in SN and VTA of mutant mice (Figure 3A, SN: wild-type 86.3 ± 1.6%, hA53T-SNCA/PINK1KO 68 ± 2%, $p<0.001$; VTA: wild-type 88.4 ± 0.9%, hA53T-SNCA/PINK1KO 70.9 ± 1.6%, $p<0.001$ and Suppl. Fig. 4A,B). Concomitantly, the percentage of DA neurons showing no nucleolar staining increased (Figure 3A SN: wild-type 9.4 ± 1.1%, hA53T-SNCA/PINK1KO 14.8 ± 1.3%, $p<0.05$; VTA: wild-type 6.2 ± 0.5%, hA53T-SNCA/PINK1KO 13.5 ± 1.6%, $p<0.05$). Nevertheless, the percent of TH positive neurons with more than one 47S signal was also increased in the hA53T-SNCA/PINK1KO mutant mice, suggesting that in a subset of DA neurons transcription of rDNA was promoted (Figure 3A SN: wild-type 4.3 ± 0.8%, hA53T-SNCA/PINK1KO 17 ± 3%, $p<0.01$; VTA: wild-type 5.3 ± 0.7%, hA53T-SNCA/PINK1KO 15.5 ± 1.1%, $p<0.001$). These data were supported by IHC with NCL and nucleophosmin/B23 (NPM) specific antibodies in combination with TH (Figures 3B-D). Analysis of the distribution of these two independent nucleolar markers in TH-positive neurons showed that the number of neurons containing two or three nucleoli was significantly higher in the hA53T-SNCA/PINK1KO mutant mice (Figures 3C,D and Suppl. Fig. 4C-F). This pattern of staining might suggest the activation of compensatory mechanisms promoting nucleolar activity in young mice.

To further explore the hypothesis that reduced levels of 47S pre-rRNA and altered nucleolar integrity at late stages could be linked to reduced expression of rRNA synthesis regulators, we analyzed by qRT-PCR, the levels of NCL and NPM/B23 mRNA, nucleolar proteins known to play a role in the regulation of rRNA synthesis, in the ventral midbrain samples from hA53T-SNCA/PINK1KO mice and age-matched controls at 3, 16 and 18 months

(Figure 3E and Suppl. Fig. 4G,H). No differences were detected, suggesting that impaired nucleolar activity observed by qRT-PCR and by ISH was not linked to a general transcriptional deficit in the ventral midbrain.

Interestingly, TIF-IA mRNA levels were significantly lower in the ventral midbrain of human *post mortem* PD brain samples compared to those from matched controls (N=8 control and N=5, PD) (Figure 4A). These findings would support previous evidence of impaired rRNA synthesis in PD symptomatic stages (Kang and Shin, 2014, Rieker et al., 2011), however they need to be interpreted with caution given the different cellular composition of the human ventral midbrain tissue in control and PD patients. To further investigate a link between PD-related mutations and nucleolar activity in hA53T-SNCA/PINK1KO models, we analyzed the expression of TIF-IA in hA53T-SNCA/PINK1KO mice Similar as in the human PD samples, TIF-IA mRNA in ventral midbrain tissue was reduced at a clearly symptomatic stage (18 months) - surprisingly after a transitory upregulation phase (Figure 4B at 16 months: wild-type 1.00 ± 0.04, hA53T-SNCA/PINK1KO 1.47 ± 0.14, $p<0.05$; at 18 months: wild-type 1.00 ± 0.02, hA53T-SNCA/PINK1KO 0.862 ± 0.015, $p<0.05$ and Suppl. Fig. 5).

**rDNA transcription is unaltered in a pre-symptomatic PD model based on the genetic inactivation of DJ-1 and PINK1.**

Similarly, we analyzed nucleolar activity in genetic models of pre-symptomatic PD based on autosomal recessive PARK gene mutations. Parkin mutant mice have been previously analyzed (Kang and Shin, 2014). Here we focused on DJ-1/PINK1 double knock-out (DKO) mice and control littermates. By qRT-PCR analysis of pre-rRNA (+1/+130) and the intermediate precursor (+597/+765) were similar in dissected ventral midbrain samples from adult control, PINK1$^{-/-}$ and in DKO mice (here 7 month-old) (Figure 5A and Suppl. Fig. 6A).

The quantitative analysis of 47S pre-rRNA signal in DA neurons after *in situ* hybridization in combination with TH immunostaining did not reveal a decreased stained area in TH positive neurons of DJ-1$^{-/-}$, PINK1$^{-/-}$ and DKO mice, further supporting the conclusion that the loss of both DJ-1 and PINK1 did not impair rDNA transcription (Figure 5B,C). On the contrary, the stained area identifying the nucleolar 47S signal in SN DA neurons of DKO mice, was significantly larger than that of controls, while the other differences did not reach statistical significance (Figure 5C, SN: wild-type 1.00 ±0.04, DJ1 KO 1.34±0.04, PINK1 KO 1.40 ± 0.11, DKO 1.45 ± 0.13, $p=0.031$ for wild-type vs DKO, $p=0.107$ for wild-type vs DJ-1 KO, $p=0.053$ for wild-type vs PINK1 KO; VTA: wild-type 1.00 ±0.10, DJ1 KO 1.31±0.19, PINK1 KO 1.35 ± 0.16, DKO 1.29 ± 0.10, $p=0.282$ for wild-type vs DJ-1 KO, $p=0.197$ for

wild-type vs PINK1 KO, p=0.335 for wild-type vs DKO and Suppl. Fig. 6B). The analysis of NCL, NPM and TIF-IA mRNA levels in ventral midbrain from control, PINK1 KO and DJ-1/PINK1 DKO mice did not show any significant difference (Figure 5D and Suppl. Fig. 6C). These results indicate that pre-symptomatic PD models activate compensatory transcriptional mechanisms maintaining RNA Polymerase I activity, however symptomatic stages are in general associated with disrupted nucleolar function and integrity (Rieker et al., 2011).

**Early PD-like phenotypes caused by TIF-IA loss are not enhanced by DJ-1/PINK1-dependent networks.**

These results indicated that differently from the hA53T-SNCA/PINK1KO and from the previously reported neurotoxin-based models (Healy-Stoffel et al., 2013, Rieker et al., 2011), loss of DJ-1 and PINK1 did not impair nucleolar activity in DA neurons.

The observation that DA-specific TIF-IA conditional KO mice (cKO) are more vulnerable to acute MPTP treatment suggested the interaction of nucleolar- and mitochondrial-dependent pathways in these models of neurodegeneration (Rieker et al., 2011). Along the same line, because both DJ-1 and PINK1 play a neuroprotective role against oxidative stress, here we tested the hypothesis that lack of DJ-1/PINK1 KO could exacerbate the effects of nucleolar stress in DA neurons, suggesting that the pathways regulated by DJ-1/PINK1 interact with those triggered by nucleolar stress.

To this end we generated inducible DA TIF-IA cKO mice lacking DJ-1 and PINK1 genes (triple KO, TKO) and we analyzed them at age 3 months, and 7 weeks after tamoxifen injection, a stage at which no significant neuronal death had occurred yet in the DA TIF-IA cKO mice (Rieker et al., 2011) (Figure 6A). First, we confirmed that nucleolar integrity was disrupted in DA neurons of TIF-IA cKO and TKO by confocal analysis of immunofluorescent stainings with NCL and TH specific antibodies (Figure 6B). Similarly, we showed that NCL distribution was unaltered in the DJ-1/PINK1 DKO mice. Moreover, the induction of nucleolar stress in DA neurons was confirmed by IHC showing increased p53 protein levels in TKO mice (Figure 6C), as p53 levels are known to increase as a result of nucleolar stress (Rieker et al., 2011).

However, TH immunoreactivity in the striatum of cKO and TKO was comparable indicating that loss of DJ-1/PINK1 does not exacerbate the toxic effects of nucleolar stress (Figure 6D, E; wild-type 100 ± 15%, DKO 121 ± 15%, cKO 63 ± 15%, TKO 45 ± 6%, $p<0.05$ for wild-type vs TKO, $p<0.01$ for DKO vs TKO and Suppl. Fig. 7A). These results were supported by the comparable levels of dopamine in the striata of TIF-IA cKO and TKO mice measured by

high-performance liquid chromatography followed by electrochemical detection (HPLC-ED) (Figure 6F, wild-type 16.3 ± 1.7 ng/mg, DKO 22 ± 2 ng/mg, cKO 5.7 ± 0.2 ng/mg, TKO 8.6 ± 1.0 ng/mg, $p<0.05$ for wild-type vs cKO, $p<0.01$ for DKO vs TKO, $p<0.001$ for DKO vs cKO and Suppl. Fig. 7B). In summary, the results for the DKO and TKO indicate that loss of DJ-1/PINK1 does not impair nucleolar activity and integrity in a pre-symptomatic stage, while in contrast to the hA53T-SNCA/PINK1KO.

## MATERIALS AND METHODS

### Statement regarding the ethical use of human material and animals

Procedures involving animal care were approved by the Committee on Animal Care and Use (Regierungspräsidium Karlsruhe, 35-9185.81/G- 180/08) in accordance with the local Animal Welfare Act and the European Communities Council Directives (2010/63/EU and 2012/707/EU). Human postmortem midbrain tissue blocks were provided by the German BrainNet, Grant-No. GA 28, for details of samples, please see (Schlaudraff et al., 2014).

### Human samples

Detailed information on the 13 human postmortem ventral midbrain tissues from controls and PD brains can be found in Schlaudraff et al., 2014 (Schlaudraff et al., 2014). Mean age of controls (N=8) 69±1.6 years and PDs (N=5) 78.2±1.3 years (Braak stages 0, II, III, IV, V).

### Mice

DJ1$^{-/-}$ and PINK1$^{-/-}$ mice in a C57Bl6/J background were generously donated by Dr. Wolfgang Wurst (Helmholtz Zentrum München, Neuherberg, Germany) (Pham et al., 2010, Glasl et al., 2012).

Homozygous TIF-IA$^{flox/flox}$; DATCreERT2 mutant mice were generated by crossing mice carrying the *TIF-IA* floxed allele (TIF-IA$^{flox/flox}$) to the transgenic line DATCreERT2. TIF-IA$^{+/flox}$; DATCreERT2 positive mice were again crossed with TIF-IA$^{flox/flox}$ mice. The analysis of the genotype was performed as previously described (Rieker et al., 2011). These mice were crossed to DJ1$^{-/-}$ and PINK1$^{-/-}$ double knock-out mice to obtain triple knock out mice that lack TIF-IA in DA neurons after tamoxifen induction of CreERT2. To induce TIF-IA gene deletion in DA neurons, 2 month-old mice were injected intraperitoneally with 1 mg tamoxifen (TAM) twice a day for five consecutive days and were analyzed 7 weeks after the last injection (Rieker et al., 2011). As controls, littermates with wild type allele for all genes also injected with tamoxifen were examined. Both male and female mice were used for the experiments. PrPmtA mice overexpressing the human A53T-SNCA mutation were crossed with PINK1$^{-/-}$ mice, as previously described (Gispert et al., 2015). For the experiments reported here, male and female mice were used.

**Histological analysis**

Mice were sacrificed by cervical dislocation and brains were immediately dissected. For immunohistochemistry, one brain hemisphere was fixed in 4% paraformaldehyde overnight and paraffin embedded or sectioned on a vibratome (50 µm thickness), while paraffin sections were 7 µm thick. Vibratome sections containing the striatum comprised between Bregma +0.14 mm and -0.98 mm and paraffin sections from the midbrain region comprised between Bregma -2.54 mm and -3.80 mm were used for the analysis and incubated with primary antibodies overnight at 4°C. Visualization of antigen-bound primary antibodies following antigen retrieval (HK086-9K, Biogenex) was carried out using a biotinylated secondary antibody together with the avidin-biotin system and the VECTOR peroxidase kit (PK-6100, Vector Laboratories) using both diaminobenzidine tablets (D4293, Sigma) and HistoGreen HRP-substrate kit (E109, Vector) as a substrate. For immunofluorescence, secondary antibodies Alexa 488 (A-21206), Alexa 594 (A-21207) and Alexa 647 (A-21448) (1:100, Thermo Scientific) were used. Primary antibodies for immunostaining were: anti-alpha-synuclein (1:500, ab27766, abcam), anti-nucleolin (1:500, ab70493, abcam), anti-nucleophosmin (1:100, MAB4500, NPM/B23) (Millipore), anti-tyrosine hydroxylase (1:500, AB1542, Millipore), anti-p53 (1:400, NCL-p53-CM5p, Novocastra).

Non-radioactive *in situ* hybridization (ISH) was performed on paraffin sections using a specific riboprobe hybridizing to regions in the leader sequence of the pre-rRNA followed by IHC with TH antibody as previously described (Rieker et al., 2011). The *in situ* hybridization signal was quantified by labeling the riboprobe with digoxigenin. This produced a defined signal area (ca. the size of nucleoli) that was used for quantification of the nucleolar area by ImageJ software (Rieker et al., 2011). For confocal analysis images were acquired by a Leica SP8 system.

**RNA isolation and qRT-PCR**

Total RNA was isolated from dissected mouse ventral midbrain in the region comprised between Bregma -2.54 mm and -3.80 mm. Levels of NCL, NPM, TIF-IA mRNA and pre-rRNA were monitored by reverse transcription (RT) followed by qRT-PCR. Synthesis of cDNA with M-MLV Reverse Transcriptase (SuperScript III First Strand Synthesis Supermix) (18080-400, Thermo Scientific) was primed with random hexamers. For detection of pre-rRNA, either the first 130 nucleotides relative to the transcription start site were amplified using the 5'-ACTGACACGCTGTCCTTTCC and 5'-GACAGCTTCAGGCACCGCGA

primers or a primer pair covering the first processing site was used: 5′-CGTGTAAGACATTCCTATCTCG and 5′- GCCCGCTGGCAGAACGAGAAG. To amplify GAPDH we used the following primers: 5′-CATGGCCTTCCGTGTTCCTA and 5′-GCGGCACGTCAGATCCA. pre-RNA levels relative to GAPDH mRNA levels were determined using SYBR GREEN chemistry (SYBR Green Mix, 04887352001, Roche) by a Light Cycler 480 instrument (Roche), as previously described (Kiryk et al, 2013). For each amplicon serial dilutions of cDNA from the ventral midbrain were included in each run to generate standard curves for relative quantification by the Light Cycler 480 instrument's software. The relative changes in pre-rRNA expression were normalized to GAPDH, as a reference gene, after checking its stable expression. The analysis of the mouse ventral midbrain cDNA was performed by a StepOnePlus instrument (Applied Biosystems). The following TaqMan gene expression assays were used: TIF-IA (Mm01344420_m1), nucleolin (Mm01290591_m1), nucleophosmin (Mm02391781_g1), and Tbp (TATA-binding protein) (Mm00446973-m1) (Applied Biosystems/Life Technologies). For the TaqMan assays the "*delta-delta CT*" (ΔΔCT) method was used to normalize the mouse qRT-PCR data by the $2^{-\Delta\Delta C_T}$ formula (Livak and Schmittgen, 2001). The normalization was performed using the stably expressed reference gene Tbp. Expression changes were calculated as a fold change versus mean of respective control samples.

Total RNA from human postmortem horizontal midbrain tissue cryosections was analyzed on an Applied Biosystems GeneAmp 7900HT PCR instrument, as previously described (Grundemann et al., 2008, Grundemann et al., 2011, Schlaudraff et al., 2014) The human TIF-IA (Hs00255800_m1) and the ENO2 (Hs00157360_m1) TaqMan assays (Applied Biosystems) were used for real-time qPCR, and expression levels were calculated using respective standard curve data by the formula $S^{[(Ct\text{-}Yintercept)/slope]}$, where S is the serial dilution factor of the standard curve. The data were calculated in respect to ENO2 (neuron specific enolase), by using slopes of respective standard curves over 4-magnitudes as described in detail in (Schlaudraff et al., 2014). We have empirically proven that ENO2 mRNA is expressed at constant levels in individual SN DA neurons (Liss et al., 2001).

**HPLC-ED**

The striatum comprised between Bregma +0.14 mm and -0.98 mm was dissected using a mouse brain matrix and dopamine content was measured per mg of wet weight (ww) by HPLC-ED as previously described (Rieker et al., 2011).

**Statistical analysis**

Eight coronal paraffin sections (every 4$^{th}$ section) per mouse were analyzed within the ventral midbrain and hippocampus for ISH and IHC. The ImageJ software was used to measure the area occupied by the 47S signal for at least 150 nucleoli per mouse. For DA neurons, the total area of the nucleolar signal per mouse was normalized to the number of TH positive neurons in either SN or VTA (at least 150 cells per mouse in SN and at least 150 cells per mouse in VTA), in this way we obtained the average 47S signal area per cell per mouse. The average area per mouse from at least 3 mice per genotype at each age was used to calculate the average nucleolar area per genotype and age. The average area per genotype was then plotted as fold change relative to the average area of the respective control and the results are expressed as the mean of the fold changes ± S.E.M. Individual data plots are included as Supplementary Figures. The ImageJ was also used to measure TH immunoreactivity in the striatum in vibratome sections (Rieker et al., 2011). All measurements were carried out at least in triplicate as specified in the figure legends Statistical significance of the results was analyzed by one-way or two-way ANOVA, followed by post-hoc tests for comparisons between multiple groups or by Student's *t* test for comparisons between two groups of values, as indicated in figure legends, using GraphPad Prism (GraphPad Software, Inc) or SPSS Statistics (IBM Corp.) software packages. In all cases, $p<0.05$ was considered significant.

## DISCUSSION

Nucleolar stress is emerging as one important factor in neurodegenerative diseases (Hetman and Pietrzak, 2012, Parlato and Bierhoff, 2015). In general, for still unclear reasons, inhibition of rRNA synthesis could be both neuroprotective and neurotoxic (Kreiner et al., 2013). Our study shows a differential effect of PD-related (PARK) genetic mutations on nucleolar activity. While hA53T-SNCA/PINK1KO did affect nucleolar activity, DJ1 (PARK7) and PINK1 (PARK6) did not. Our results also show that nucleolar activity decreases with increased phenotypic severity, reinforcing its role as a stress sensor. The localization of mutant alpha-synuclein in the nucleoli of DA neurons of hA53T-SNCA/PINK1KO mice suggests that this mutant protein may directly interfere with regulators of the RNA polymerase I transcriptional machinery. Because NCL is mainly localized in the dense fibrillar compartment where transcription and processing of rDNA take place, these steps of rRNA biogenesis might be altered in the hA53T-SNCA/PINK1KO mice (Sirri et al., 2008, Berger et al., 2015). A similar function is common to causative mutant proteins, for example, in polyglutamine diseases (Parlato and Bierhoff, 2015, Tsoi et al., 2012). However, based on this study we cannot rule out the possibility that the hA53T-SNCA mutation is responsible for the altered nucleolar activity and integrity observed at 3 and 20 months. Given the observation that the PINK1 KO mice do not show the same phenotype as the hA53T-SNCA/PINK1KO double mutants, the hA53T-SNCA mutation might account for the decreased pre-rRNA and reduced nucleolar area observed in the early symptomatic stage (from 16 months on).

The major advantage of the models examined here is that they do not show neurodegeneration, enabling to dissect the impact of specific PD mutations on nucleolar activity and integrity independently of neuronal loss. Moreover, the experimental approaches adopted here allowed to characterize rRNA synthesis in specific DA neurons at pre-symptomatic PD stages.

The altered distribution of nucleolar proteins such as NCL and NPM in hA53T-SNCA/PINK1KO mice confirms that in a subset of DA neurons nucleolar activity is downregulated and nucleolar integrity disrupted at an early stage. Intriguingly in the meantime another group of DA neurons upregulate rRNA synthesis as shown by increased number of nucleoli, supporting the hypothesis that initial compensatory mechanisms target nucleolar activity. A similar condition has been also reported in motor neurons in a murine model of ALS in response to the disturbance of endoplasmic reticulum proteostasis and in response to proteasome inhibition in sensory ganglion neurons (Palanca et al., 2014, Riancho

et al., 2014). In this regard, we should mention that the hypertrophy of cortical neurons and their nuclei and nucleoli in asymptomatic Alzheimer's disease may represent an early reaction to the presence of neurotoxic Aβ or tau, or a compensatory mechanism that prevents the progression of the disease into dementia (Iacono et al., 2008, Riudavets et al., 2007). This is linked to local Aβ-induced metabolic insults and neuronal death (Cohen et al., 2009). Our previous results show that the neuroprotective deletion of Pten in adult DA neurons also results in the increase of neuronal soma and nucleolar size (Domanskyi et al., 2011). Future studies are necessary to establish whether enhanced nucleolar activity at a pre-symptomatic stage is neuroprotective or on the other hand might even actively contribute to neurodegenerative pathways - with potential implications for design of therapeutic strategies. The next fundamental question is in fact to which extent a controlled downregulation of nucleolar function could even be beneficial under cellular stress (Mayer and Grummt, 2005). Hence, further studies are required to establish the role of the significant decrease of 47S pre-rRNA observed in the hA53T-SNCA/PINK1KO mice in VTA DA neurons. This observation suggests a differential regulation of nucleolar activity in more resistant VTA DA neurons and highly vulnerable SN DA neurons, that are the most vulnerable DA population in PD, in line with the functional and metabolic differences between VTA and SN neurons (Duda et al., 2016). Of course this differential vulnerability may simply be due to the heterologous prion promoter driving differing overexpression levels of hA53T-SNCA in the two neuronal populations. However, we cannot link this reduced nucleolar activity to a reduced neuronal survival in this model given its reduced lifespan. Ultimately the decreased pre-rRNA synthesis observed at the late stage in this model could be linked to aging and/or be a consequence of the severe synaptic deficits in these mice (Johnson et al., 1998, Burke, 2010). Future studies in other mouse models generated by a knock-in approach and expressing different point mutations in the human alpha-synuclein gene that lead to familial PD forms, like A30P, could provide further help to define in detail the link between specific PD-mutations and nucleolar activity (Plaas et al., 2008, Antony et al., 2011).

Differently from dominant negative mutant forms of alpha-synuclein, DJ-1 and PINK1 loss-of-function mutations do not impair rDNA transcription in DA neurons. However, the DJ-1 L166P mutation that results in misfolded DJ-1 proteins with gain-of function effects, leads to an increase of rDNA transcription in SH-SY5Y cells upon proteasome inhibition differently from DJ-1 loss-of-function mutation that has no effect (Vilotti et al., 2012). Loss of DJ-1 has been shown to induce fragmentation of mitochondria and to cause a deficit in mitochondrial fusion resulting in increased endogenous oxidative stress (Pham et al., 2010). Similarly PINK1 loss influences cellular sensitivity to toxins protecting against mitochondrial fragmentation (Glasl et al., 2012). Drosophila PINK1 mutants show global downregulation of translation, suggesting that such cellular response compensates mitochondrial dysfunction by limiting energy consumption. In fact enhanced translation through S6 kinase activation significantly exacerbated PINK1 mutant phenotypes, whereas reduction of translation suppressed the phenotype (Liu and Lu, 2010). Based on the observation that loss of TIF-IA results in downregulation of mTOR activity, impaired mitochondrial activity and increased oxidative stress (Rieker et al., 2011, Kreiner et al., 2013), we expected an exacerbated impact of nucleolar stress in DA neurons lacking DJ-1/PINK1 in particular on DA striatal projections and dopamine content. However, the results of this study may indicate that DJ-1 and PINK1 may function either upstream or independently of the rRNA control pathway, or that they trigger protective compensatory processes that lead to normal nucleolar function at pre-symptomatic stages.

The current link between PD-related mutations and rDNA synthesis regulators, such as NCL, NPM and TIF-IA is further summarized in Table 1. The expression levels of NCL are dramatically reduced in the SN of human PD subjects, compared with controls (Caudle et al., 2009) as well as those of TIF-IA and could account for the reduced rRNA synthesis in PD. NCL but also NPM/B23 may play a role in rRNA synthesis and in neuronal survival (Pfister and D'Mello, 2015), prompting to assume an important role of nucleolin also in PD by regulation of rRNA synthesis. Evidence of reduced NPM/B23 in PD has been also recently provided (Garcia-Esparcia et al., 2015). Interestingly both DJ-1 and alpha-synuclein associate with NCL, hence an imbalance in this interaction could as well alter rRNA synthesis (Jin et al., 2007). We could not detect any change in NCL mRNA in all genetic pre-symptomatic PD mouse models, however NCL and alpha-synuclein colocalize in hA53T-SNCA/PINK1KO, suggesting that NCL could be responsible for the observed changes in rRNA synthesis in these mutants through a yet to be elucidated mechanism. Further studies should address

whether these mechanisms targeting the nucleolus occur in pre-symptomatic PD and in other genetic PD models. Mostly it would be important to establish whether and when changes of nucleolar activity turn to be fatal, what triggers them and why they have a cell-specific impact.

Conditional loss of Parkin in DA neurons has been shown to downregulate rRNA synthesis (Kang and Shin, 2014). NPM and NCL interact with PARIS (PARkin Interacting Substrate, ZNF746) and PARIS co-localizes with parkin in the nucleolus (Kang and Shin, 2014). Interestingly overexpression of PARIS inhibits rRNA synthesis resulting in ca. 30% less pre-rRNA three months after induction of the mutation. The same study shows that PARIS protein levels increases also in PD patients and that 47S pre-rRNA is reduced in the SN of PD patients.

There is growing evidence that DJ-1, PINK1 and parkin interact with each other, in particular PINK1 phosphorylates and activates parkin and DJ-1 physically interacts with the transcription factor forkhead box O3a, Foxo3a, to activate the *Pink1* promoter in DJ-1 KO mouse embryonic fibroblasts (Requejo-Aguilar et al., 2015). However differently from parkin cKO mice showing neurodegeneration at later stages, but also differently from PD and neurotoxin-based models (Rieker et al., 2011, Garcia-Esparcia et al., 2015), RNA polymerase I activity is not severely impaired in hA53T-SNCA/PINK1KO, PINK1 KO and in DJ-1/PINK1 DKO mice supporting the hypothesis that compensatory responses might sustain nucleolar activity (Mullin and Schapira, 2015). Understanding these complex mechanisms is the prerequisite for novel neuroprotective strategies, based on selective modulation of nucleolar function.

**Acknowledgements**

We thank Prof. G. Auburger for his insightful discussions and critical reading of the manuscript, Prof. J. Kirsch for providing suggestions and infrastructure to perform confocal analysis and imaging, Prof. G. Schütz for his support with the project. We thank R. Hertel and R. Aldaher for assistance with HPLC-ED and microscopic analysis, S. Spieth for her help with genotyping, M. Fauler for help with human data analysis. We also thank Neuroscience Master students of the Heidelberg Lab-Rotation Program supporting part of the experiments.

**Competing interests**

No competing interest declared.

**Author contributions**

VE, HB, AD performed and analyzed most of the experiments and contributed to write the manuscript, SG performed experiments and provided mouse models, RM performed immunofluorescence experiments, FS performed analysis of human PD samples, BL analyzed experiments and wrote the manuscript, RP conceived the study, analyzed experiments and wrote the manuscript.

**Funding**

The work was supported by the German Federal Ministry for Education and Research (BMBF) through NGFNplus grant FZK 01GS08142 (G. Schütz) and 01GS08141, the Alfried Krupp Prize and the DFG LI 1754/1-2 (BL). RP is supported by the German Research Foundation through the DFG PA 1529/2-1 grant.

**List of symbols and abbreviations**

ALS/FTD: amyotrophic lateral sclerosis and fronto-temporal dementia

cKO: DA-specific TIF-IA conditional KO mice

DA: dopaminergic

ΔΔCT: delta-delta CT

DKO: double knock-out

GAPDH: glyceraldehyde 3-phosphate dehydrogenase

HPLC-ED: high-performance liquid chromatography followed by electrochemical detection

HD: Huntington´s disease

Hprt: Hypoxanthine-phophoribosyltransferase

IHC: immunohistochemistry

ISH: non-radioactive *in situ* hybridization

MPTP: *N*-methyl-4-phenyl-1,2,3,6-tetrahydropyridine

mTOR: mammalian target of rapamycin

nuc: nucleolus/i

NCL: nucleolin

NPM: nucleophosmin/B23

PARK: PD-related genes

PD: Parkinson's disease

PINK1/PARK6: PTEN-induced kinase 1

Pre-rRNA: precursor rRNA

qRT-PCR: quantitative real-time PCR

rDNA: ribosomal DNA

SN: substantia nigra

TAM: Tamoxifen

TH: tyrosine hydroxylase

Tbp: TATA-binding protein

TIF-IA: transcription initiation factor-IA

TKO: triple KO

VTA: ventral tegmental area

ww: wet weight

**References**


Antony, P. M., Diederich, N. J. & Balling, R. 2011. Parkinson's disease mouse models in translational research. *Mamm Genome,* 22**,** 401-19.

Auburger, G., Gispert, S. & Brehm, N. 2016. Methyl-Arginine Profile of Brain from Aged PINK1-KO+A53T-SNCA Mice Suggests Altered Mitochondrial Biogenesis. *Parkinsons Dis,* 2016**,** 4686185.

Berger, C. M., Gaume, X. & Bouvet, P. 2015. The roles of nucleolin subcellular localization in cancer. *Biochimie,* 113**,** 78-85.

Boulon, S., Westman, B. J., Hutten, S., Boisvert, F. M. & Lamond, A. I. 2010. The nucleolus under stress. *Mol Cell,* 40**,** 216-27.

Burke, R. E. 2010. Intracellular signalling pathways in dopamine cell death and axonal degeneration. *Prog Brain Res,* 183**,** 79-97.

Caudle, W. M., Kitsou, E., Li, J., Bradner, J. & Zhang, J. 2009. A role for a novel protein, nucleolin, in Parkinson's disease. *Neurosci Lett,* 459**,** 11-5.

Cohen, A. D., Price, J. C., Weissfeld, L. A., James, J., Rosario, B. L., Bi, W., Nebes, R. D., Saxton, J. A., Snitz, B. E., Aizenstein, H. A., et al. 2009. Basal cerebral metabolism may modulate the cognitive effects of Abeta in mild cognitive impairment: an example of brain reserve. *J Neurosci,* 29**,** 14770-8.

Dawson, T. M., Ko, H. S. & Dawson, V. L. 2010. Genetic animal models of Parkinson's disease. *Neuron,* 66**,** 646-61.

Domanskyi, A., Geissler, C., Vinnikov, I. A., Alter, H., Schober, A., Vogt, M. A., Gass, P., Parlato, R. & Schutz, G. 2011. Pten ablation in adult dopaminergic neurons is neuroprotective in Parkinson's disease models. *FASEB J,* 25**,** 2898-910.

Duda, J., Potschke, C. & Liss, B. 2016. Converging roles of ion channels, calcium, metabolic stress, and activity-pattern of substantia nigra dopaminergic neurons in health and Parkinson's disease. *J Neurochem.*

Garcia-Esparcia, P., Hernandez-Ortega, K., Koneti, A., Gil, L., Delgado-Morales, R., Castano, E., Carmona, M. & Ferrer, I. 2015. Altered machinery of protein synthesis is region- and stage-dependent and is associated with alpha-synuclein oligomers in Parkinson's disease. *Acta Neuropathol Commun,* 3**,** 76.

Gispert, S., Brehm, N., Weil, J., Seidel, K., Rub, U., Kern, B., Walter, M., Roeper, J. & Auburger, G. 2015. Potentiation of neurotoxicity in double-mutant mice with Pink1 ablation and A53T-SNCA overexpression. *Hum Mol Genet,* 24**,** 1061-76.

Gispert, S., Del Turco, D., Garrett, L., Chen, A., Bernard, D. J., Hamm-Clement, J., Korf, H. W., Deller, T., Braak, H., Auburger, G., et al. 2003. Transgenic mice expressing mutant A53T human alpha-synuclein show neuronal dysfunction in the absence of aggregate formation. *Mol Cell Neurosci,* 24**,** 419-29.

Glasl, L., Kloos, K., Giesert, F., Roethig, A., Di Benedetto, B., Kuhn, R., Zhang, J., Hafen, U., Zerle, J., Hofmann, A., et al. 2012. Pink1-deficiency in mice impairs gait, olfaction and serotonergic innervation of the olfactory bulb. *Exp Neurol,* 235**,** 214-27.

Grummt, I. 2013. The nucleolus-guardian of cellular homeostasis and genome integrity. *Chromosoma,* 122**,** 487-97.

Grundemann, J., Schlaudraff, F., Haeckel, O. & Liss, B. 2008. Elevated alpha-synuclein mRNA levels in individual UV-laser-microdissected dopaminergic substantia nigra neurons in idiopathic Parkinson's disease. *Nucleic Acids Res,* 36**,** e38.

Grundemann, J., Schlaudraff, F. & Liss, B. 2011. UV-laser microdissection and mRNA expression analysis of individual neurons from postmortem Parkinson's disease brains. *Methods Mol Biol,* 755**,** 363-74.

Healy-Stoffel, M., Ahmad, S. O., Stanford, J. A. & Levant, B. 2013. Altered nucleolar morphology in substantia nigra dopamine neurons following 6-hydroxydopamine lesion in rats. *Neurosci Lett,* 546**,** 26-30.

Hetman, M. & Pietrzak, M. 2012. Emerging roles of the neuronal nucleolus. *Trends Neurosci,* 35**,** 305-14.

Iacono, D., O'brien, R., Resnick, S. M., Zonderman, A. B., Pletnikova, O., Rudow, G., An, Y., West, M. J., Crain, B. & Troncoso, J. C. 2008. Neuronal hypertrophy in asymptomatic Alzheimer disease. *J Neuropathol Exp Neurol,* 67**,** 578-89.

Jin, J., Li, G. J., Davis, J., Zhu, D., Wang, Y., Pan, C. & Zhang, J. 2007. Identification of novel proteins associated with both alpha-synuclein and DJ-1. *Mol Cell Proteomics,* 6**,** 845-59.

Johnson, F. B., Marciniak, R. A. & Guarente, L. 1998. Telomeres, the nucleolus and aging. *Curr Opin Cell Biol,* 10**,** 332-8.

Kang, H. & Shin, J. H. 2014. Repression of rRNA transcription by PARIS contributes to Parkinson's disease. *Neurobiol Dis,* 73C**,** 220-228.

Kim, R. H., Smith, P. D., Aleyasin, H., Hayley, S., Mount, M. P., Pownall, S., Wakeham, A., You-Ten, A. J., Kalia, S. K., Horne, P., et al. 2005. Hypersensitivity of DJ-1-deficient mice to 1-methyl-4-phenyl-1,2,3,6-tetrahydropyrindine (MPTP) and oxidative stress. *Proc Natl Acad Sci U S A,* 102**,** 5215-20.

Kitada, T., Tong, Y., Gautier, C. A. & Shen, J. 2009. Absence of nigral degeneration in aged parkin/DJ-1/PINK1 triple knockout mice. *J Neurochem,* 111**,** 696-702.

Kreiner, G., Bierhoff, H., Armentano, M., Rodriguez-Parkitna, J., Sowodniok, K., Naranjo, J. R., Bonfanti, L., Liss, B., Schutz, G., Grummt, I., et al. 2013. A neuroprotective phase precedes striatal degeneration upon nucleolar stress. *Cell Death Differ,* 20**,** 1455-1464.

Kumaran, R. & Cookson, M. R. 2015. Pathways to Parkinsonism Redux: convergent pathobiological mechanisms in genetics of Parkinson's disease. *Hum Mol Genet,* 24**,** R32-44.

Kurz, A., Double, K. L., Lastres-Becker, I., Tozzi, A., Tantucci, M., Bockhart, V., Bonin, M., Garcia-Arencibia, M., Nuber, S., Schlaudraff, F., et al. 2010. A53T-alpha-synuclein overexpression impairs dopamine signaling and striatal synaptic plasticity in old mice. *PLoS One,* 5**,** e11464.

Liss, B., Franz, O., Sewing, S., Bruns, R., Neuhoff, H. & Roeper, J. 2001. Tuning pacemaker frequency of individual dopaminergic neurons by Kv4.3L and KChip3.1 transcription. *EMBO J,* 20**,** 5715-24.

Liu, S. & Lu, B. 2010. Reduction of protein translation and activation of autophagy protect against PINK1 pathogenesis in Drosophila melanogaster. *PLoS Genet,* 6**,** e1001237.

Livak, K. J. & Schmittgen, T. D. 2001. Analysis of relative gene expression data using real-time quantitative PCR and the 2(-Delta Delta C(T)) Method. *Methods,* 25**,** 402-8.

Mayer, C. & Grummt, I. 2005. Cellular stress and nucleolar function. *Cell Cycle,* 4**,** 1036-8.

Mullin, S. & Schapira, A. 2015. The genetics of Parkinson's disease. *Br Med Bull,* 114**,** 39-52.

Narendra, D. P., Jin, S. M., Tanaka, A., Suen, D. F., Gautier, C. A., Shen, J., Cookson, M. R. & Youle, R. J. 2010. PINK1 is selectively stabilized on impaired mitochondria to activate Parkin. *PLoS Biol,* 8**,** e1000298.

Palanca, A., Casafont, I., Berciano, M. T. & Lafarga, M. 2014. Reactive nucleolar and Cajal body responses to proteasome inhibition in sensory ganglion neurons. *Biochim Biophys Acta,* 1842**,** 848-59.

Parlato, R. & Bierhoff, H. 2015. Role of nucleolar dysfunction in neurodegenerative disorders: a game of genes? . *AIMS Molecular Science,* 2**,** 211-224

Parlato, R. & Kreiner, G. 2013. Nucleolar activity in neurodegenerative diseases: a missing piece of the puzzle? *J Mol Med (Berl),* 91**,** 541-7.

Parlato, R. & Liss, B. 2014. How Parkinson's disease meets nucleolar stress. *Biochim Biophys Acta,* 1842**,** 791-797.

Pfister, J. A. & D'mello, S. R. 2015. Insights into the regulation of neuronal viability by nucleophosmin/B23. *Exp Biol Med (Maywood),* 240**,** 774-86.

Pham, T. T., Giesert, F., Rothig, A., Floss, T., Kallnik, M., Weindl, K., Holter, S. M., Ahting, U., Prokisch, H., Becker, L., et al. 2010. DJ-1-deficient mice show less TH-positive neurons in the ventral tegmental area and exhibit non-motoric behavioural impairments. *Genes Brain Behav,* 9**,** 305-17.

Plaas, M., Karis, A., Innos, J., Rebane, E., Baekelandt, V., Vaarmann, A., Luuk, H., Vasar, E. & Koks, S. 2008. Alpha-synuclein A30P point-mutation generates age-dependent nigrostriatal deficiency in mice. *J Physiol Pharmacol,* 59**,** 205-16.

Requejo-Aguilar, R., Lopez-Fabuel, I., Jimenez-Blasco, D., Fernandez, E., Almeida, A. & Bolanos, J. P. 2015. DJ1 represses glycolysis and cell proliferation by transcriptionally up-regulating Pink1. *Biochem J,* 467**,** 303-10.

Riancho, J., Ruiz-Soto, M., Villagra, N. T., Berciano, J., Berciano, M. T. & Lafarga, M. 2014. Compensatory Motor Neuron Response to Chromatolysis in the Murine hSOD1(G93A) Model of Amyotrophic Lateral Sclerosis. *Front Cell Neurosci,* 8**,** 346.

Rieker, C., Engblom, D., Kreiner, G., Domanskyi, A., Schober, A., Stotz, S., Neumann, M., Yuan, X., Grummt, I., Schutz, G., et al. 2011. Nucleolar disruption in dopaminergic neurons leads to oxidative damage and parkinsonism through repression of mammalian target of rapamycin signaling. *J Neurosci,* 31**,** 453-60.

Riudavets, M. A., Iacono, D., Resnick, S. M., O'brien, R., Zonderman, A. B., Martin, L. J., Rudow, G., Pletnikova, O. & Troncoso, J. C. 2007. Resistance to Alzheimer's pathology is associated with nuclear hypertrophy in neurons. *Neurobiol Aging,* 28**,** 1484-92.

Schlaudraff, F., Grundemann, J., Fauler, M., Dragicevic, E., Hardy, J. & Liss, B. 2014. Orchestrated increase of dopamine and PARK mRNAs but not miR-133b in dopamine neurons in Parkinson's disease. *Neurobiol Aging,* 35**,** 2302-15.

Sirri, V., Urcuqui-Inchima, S., Roussel, P. & Hernandez-Verdun, D. 2008. Nucleolus: the fascinating nuclear body. *Histochem Cell Biol,* 129**,** 13-31.

Tsoi, H., Lau, T. C., Tsang, S. Y., Lau, K. F. & Chan, H. Y. 2012. CAG expansion induces nucleolar stress in polyglutamine diseases. *Proc Natl Acad Sci U S A,* 109**,** 13428-33.

Vilotti, S., Codrich, M., Dal Ferro, M., Pinto, M., Ferrer, I., Collavin, L., Gustincich, S. & Zucchelli, S. 2012. Parkinson's Disease DJ-1 L166P Alters rRNA Biogenesis by Exclusion of TTRAP from the Nucleolus and Sequestration into Cytoplasmic Aggregates via TRAF6. *PLoS One,* 7**,** e35051.

**Figures**

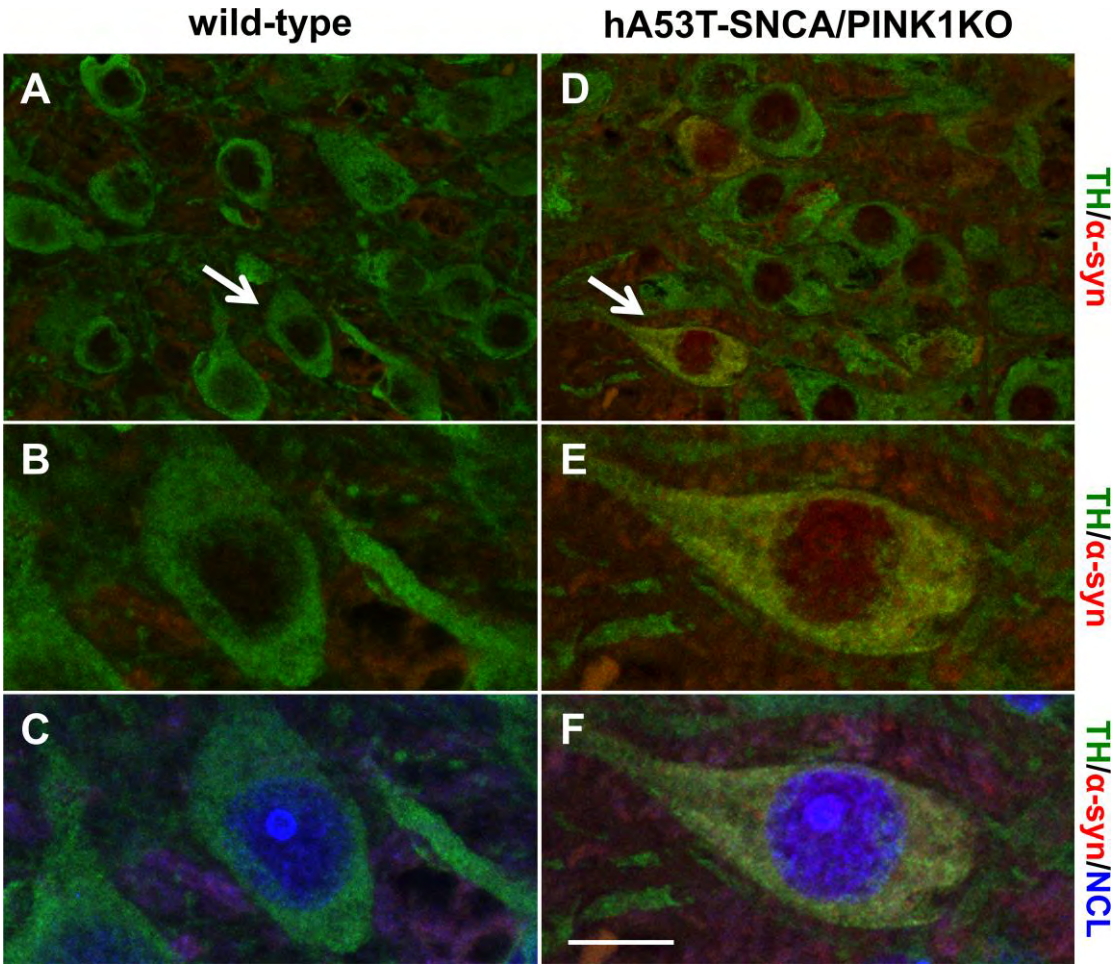


**Figure 1: hA53T-SNCA is expressed in DA neurons in the cytoplasm, the nucleus and the nucleolus.** Representative confocal microscopy images of paraffin sections immunostained with TH (green), human alpha-synuclein (red) and NCL (blue) specific antibodies from 3 month-old wild-type (**A-C**) and hA53T-SNCA overexpressing transgenic mice in a PINK1KO background (hA53T-SNCA/PINK1KO) (**D-F**). (**B, C**) and (**E, F**): Higher magnification of the region indicated by the arrow in (**A**) and (**D**), respectively. Scale bar: A, D, 25 µm; B-F, 12 µm.

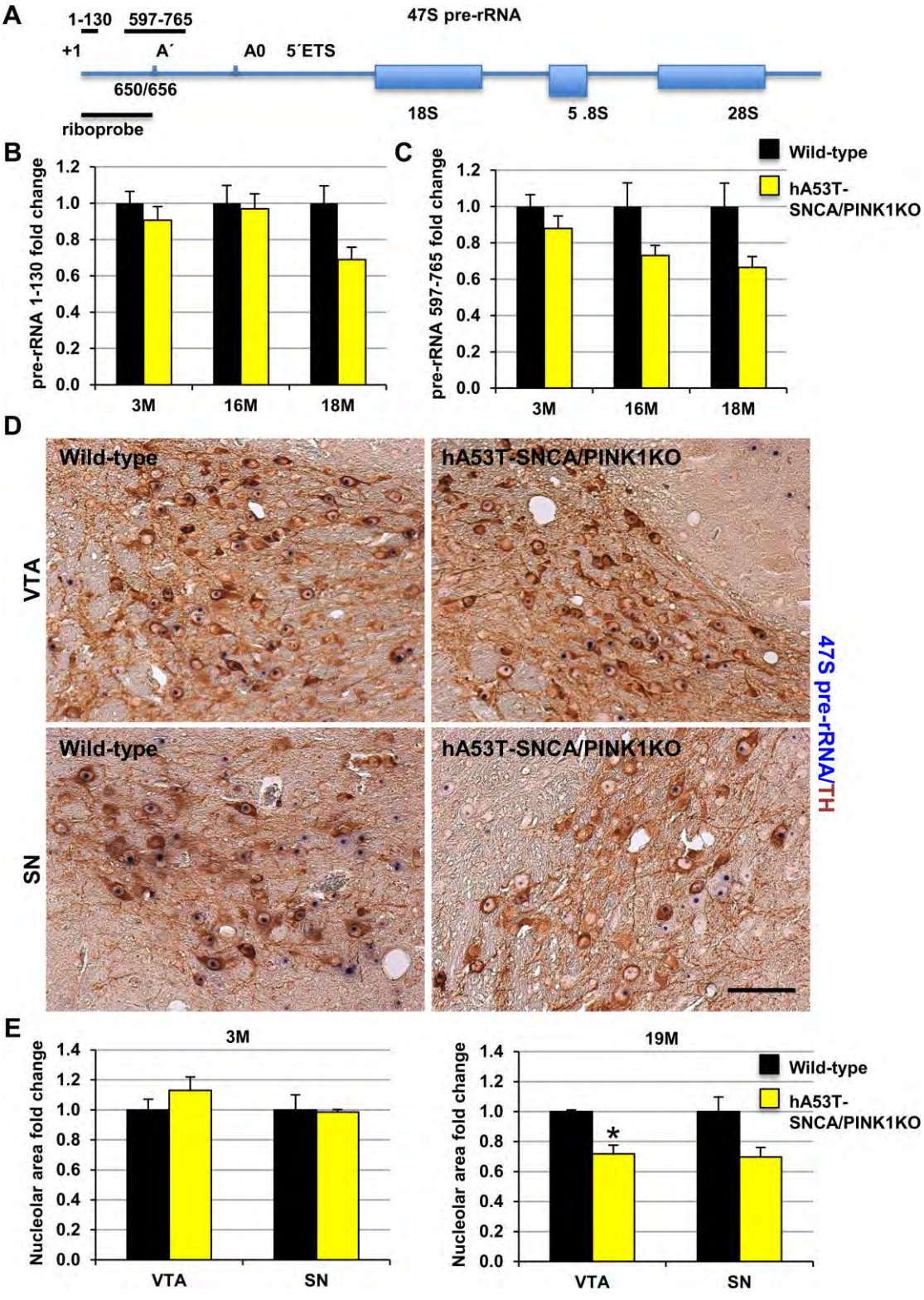
A
1-130
597-765
47S pre-rRNA
+1
A´
A0
5´ETS
650/656
18S
5 .8S
28S
riboprobe
B
pre-rRNA 1-130 fold change
1.2
1.0
0.8
0.6
0.4
0.2
0.0
3M
16M
18M
C
pre-rRNA 597-765 fold change
Wild-type
hA53T-SNCA/PINK1KO
D
VTA
SN
Wild-type
hA53T-SNCA/PINK1KO
47S pre-rRNA/TH
E
3M
19M
Nucleolar area fold change
1.4
1.2
1.0
0.8
0.6
0.4
0.2
0.0
*
VTA
SN

**Figure 2: rDNA transcription levels and reduced nucleolar area in DA neurons of hA53T-SNCA/PINK1KO mice at early symptomatic stages. A:** Schematic representation of the 47S pre-rRNA transcript including the positions of the riboprobe used for ISH, primers used for qRT-PCR and the A´ and A0 cleavage sites within the 5´ETS. **B, C:** Analysis of pre-rRNA (1-130) and pre-rRNA (597-765) by qRT-PCR at 3, 16 and 18 months in the ventral midbrain of wild-type (N=8,3,3) and hA53T-SNCA/PINK1KO mice (N=6,3,3) expressed as fold change to respective controls and normalized by GAPDH. **D:** Representative images of ISH with 47S specific riboprobe (blue) in combination with IHC by a TH specific antibody (brown) at 19 months in VTA and SN of wild-type and hA53T-SNCA/PINK1KO mice. **E:** Quantification of the area occupied by the 47S staining in hA53T-SNCA/PINK1KO expressed as fold change relative to respective controls in SN and VTA at 3 and 19 months (N=4 and 3 mice). Data are mean ± SEM; *, $p<0.05$ in comparison to wild-type mice, as determined by Student's unpaired *t*-test. Scale bar: 70 µm.

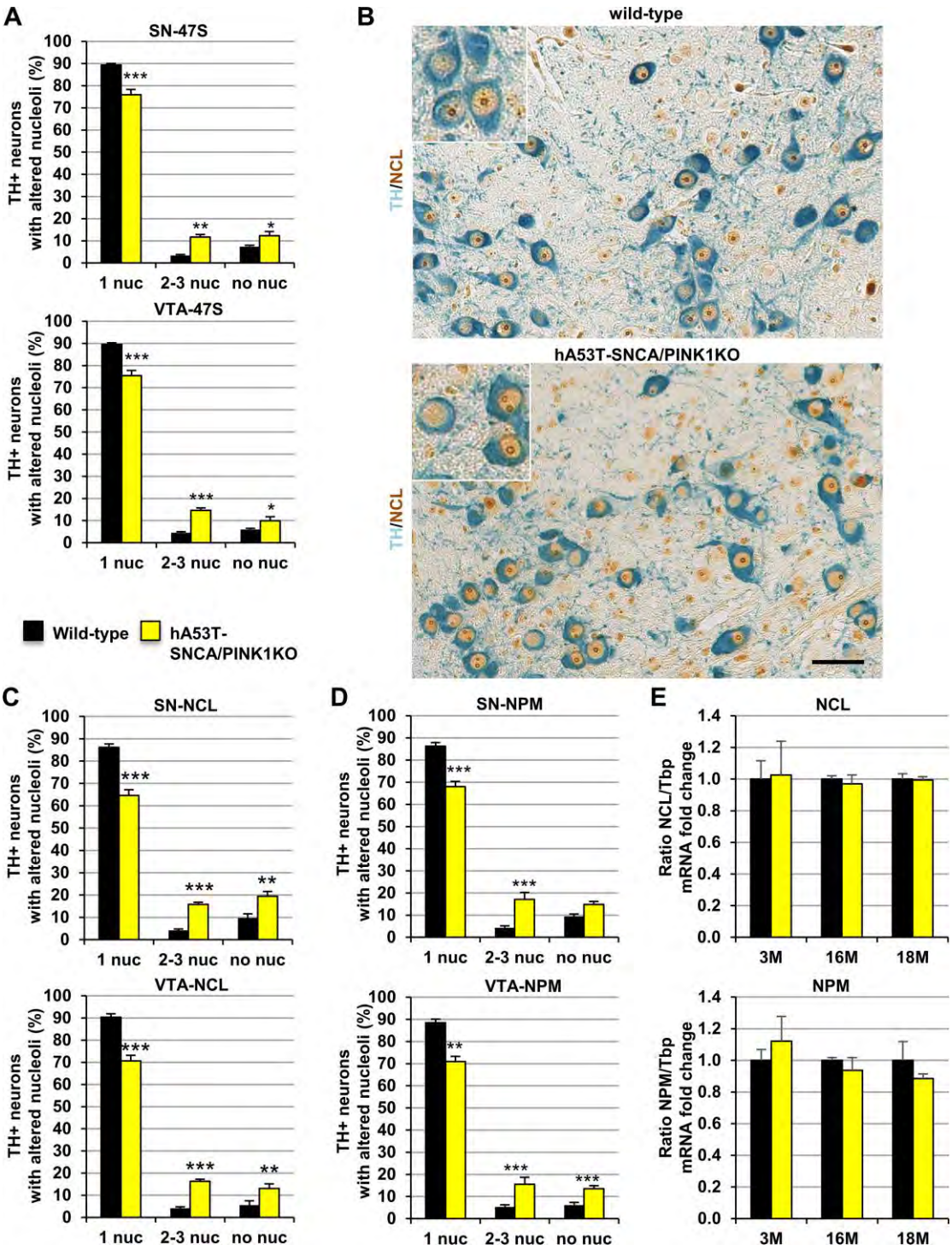
A
SN-47S
TH+ neurons with altered nucleoli (%)
1 nuc
2-3 nuc
no nuc
VTA-47S
Wild-type
hA53T-SNCA/PINK1KO
B
wild-type
TH/NCL
hA53T-SNCA/PINK1KO
C
SN-NCL
VTA-NCL
D
SN-NPM
VTA-NPM
E
NCL
Ratio NCL/Tbp mRNA fold change
NPM
Ratio NPM/Tbp mRNA fold change
3M
16M
18M

**Figure 3: Nucleolar number is altered in hA53T-SNCA/PINK1KO mice at pre-symptomatic stages. A:** Quantification of the number of nucleoli detected by ISH with 47S specific riboprobe in TH positive neurons of 3 months old wild-type and hA53T-SNCA/PINK1KO mice (N=4) in SN (left) and VTA (right) expressed as percentage of TH positive neurons with 1, 2-3 or no nucleoli. **B:** Representative images of ventral midbrain paraffin sections from 3 months-old wild-type and hA53T-SNCA/PINK1KO mice immunostained with NCL (brown) and TH (blue) specific antibodies. **C, D**: Quantification of the number of nucleoli detected by NCL (**C**) and NPM (**D**) immunostaining in TH positive neurons of wild-type and hA53T-SNCA/PINK1KO mice in SN (top) and VTA (bottom) expressed as percent of TH positive neurons with 1, 2-3 or no nucleoli (N=4 mice). **E:** Analysis of NCL (top) and NPM (bottom) mRNA levels by qRT-PCR at 3, 16 and 18 months in wild type (N=5,3,3) and hA53T-SNCA/PINK1 KO mice (N=6,3,3) expressed as fold change to respective controls and normalized by Tbp. All data are mean ± SEM; *, $p<0.05$; **, $p<0.01$; ***, $p<0.001$ in comparison to wild-type, as determined by two-way ANOVA followed by Sidak's multiple comparison test. Scale bar: 50 µm; nuc: nucleolus.

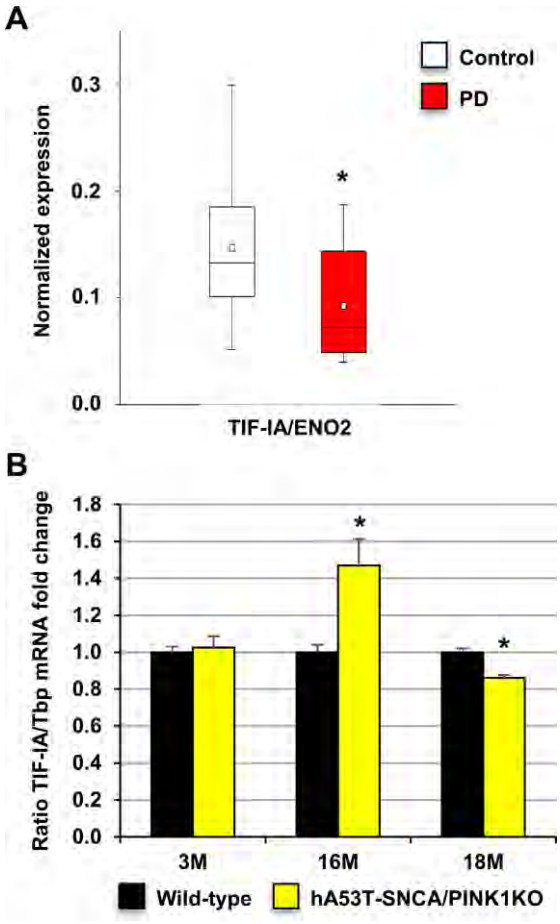


**Figure 4: Expression of TIF-IA regulating rRNA synthesis in PD patients and hA53T-SNCA/PINK1KO mice**. **A:** TIF-IA expression in ventral midbrain DA neurons in brain autopsies from PD patients (N=5, n=20 sections) and age-matched controls (N=8, n=16 sections) expressed as fold change to controls normalized by ENO2; *, p=0.0192, as determined by Wilcoxon rank sum test. **B:** Analysis of TIF-IA expression by qRT-PCR in 3, 16 and 18 months old wild-type (N=8,3,3) and hA53T-SNCA/PINK1KO mice (N=6,3,3) expressed as fold change to respective controls normalized by Tbp. Data are mean ± SEM; *, $p<0.05$ in comparison to wild-type mice, as determined by Student's unpaired *t*-test.

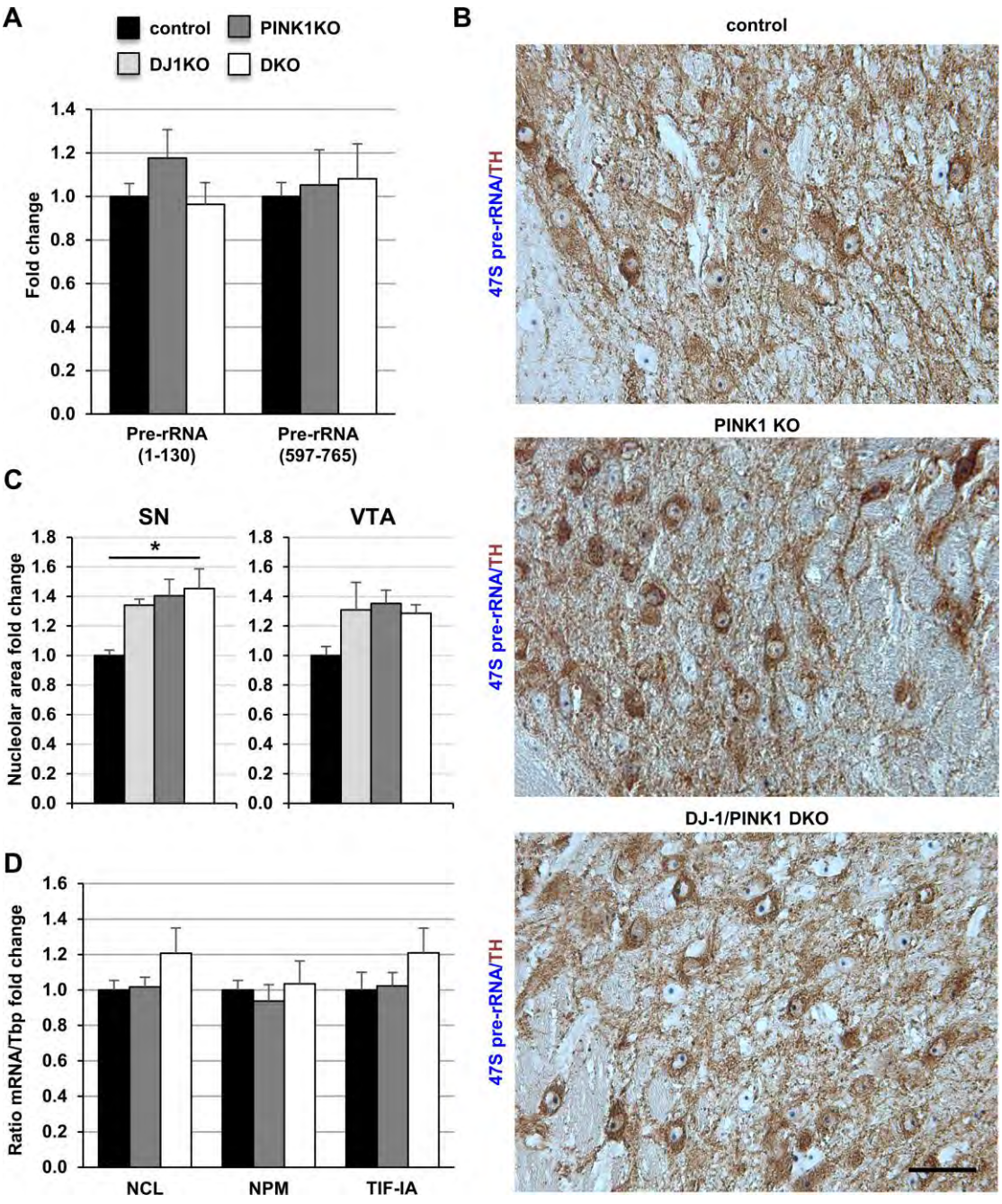

**Figure 5: rDNA transcription is not reduced in PINK1 KO and in DJ-1/PINK1 DKO mice. A:** Analysis of pre-rRNA (1-130) and pre-rRNA (597-765) by qRT-PCR in controls (N=3), PINK1 KO (N=8) and DJ-1/PINK1 DKO mice (N=8) expressed as fold change to respective controls normalized by GAPDH. **B:** Representative images of ISH with 47S specific riboprobe (blue) in combination with immunohistochemistry by a TH specific antibody (brown) in 9 months old control, PINK1 KO and DKO mice. **D:** Quantification of the area occupied by the 47S staining in control, DJ-1 KO, PINK1 KO and DKO mice expressed as fold change relative to respective controls in SN and VTA (N=3 mice). **C:** Analysis of NCL, NPM and TIF-IA mRNA levels by qRT-PCR in wild-type (N=3), PINK1 KO (N=8) and DJ-1/PINK1 DKO (N=8) mice at 9 months expressed as fold change to respective controls normalized by Tbp. All data are mean ± SEM; *, $p<0.05$ as determined by one-way ANOVA followed by Tukey's multiple comparisons test. Scale bar: 50 µm.

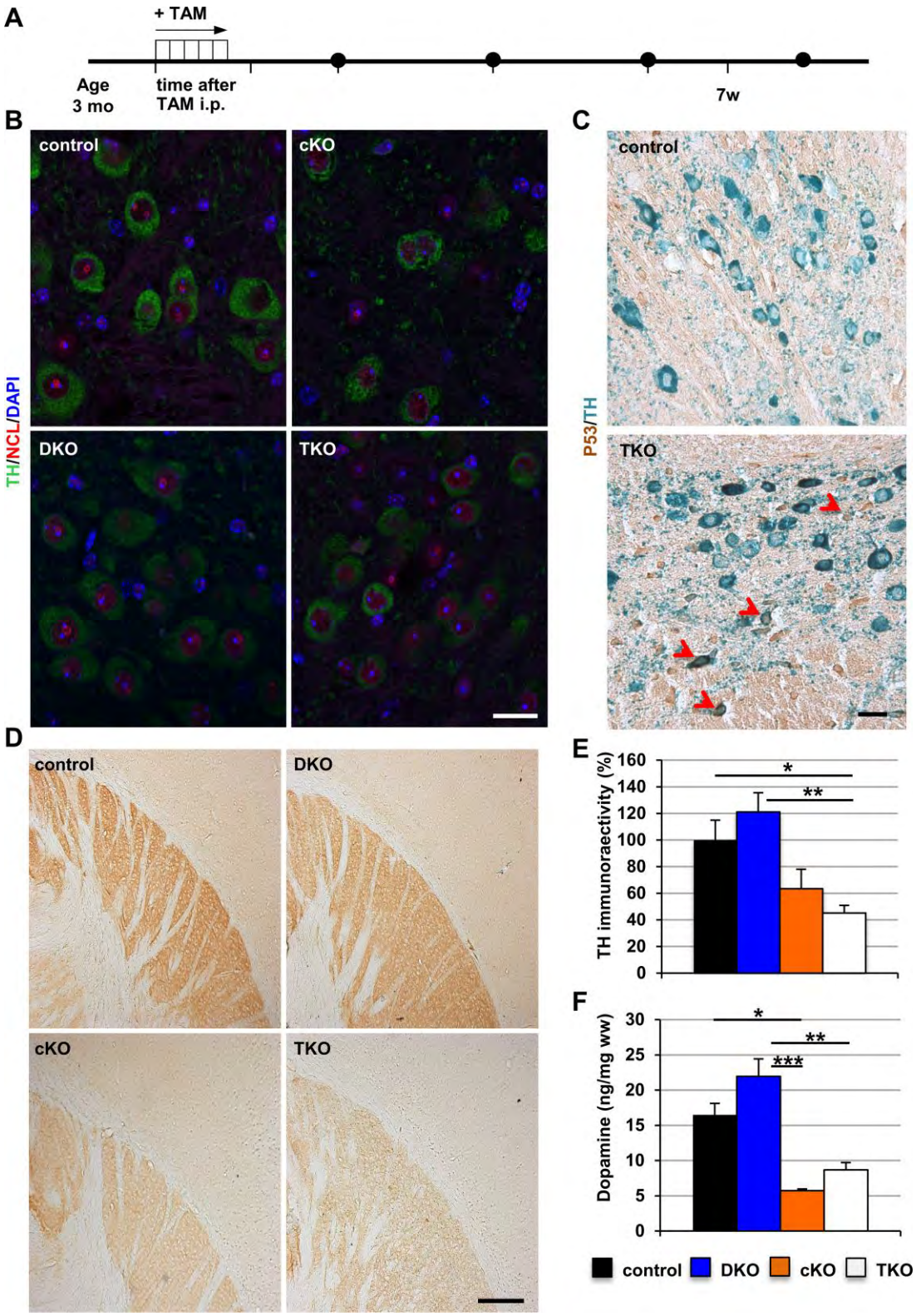
A
+ TAM
Age
3 mo
time after
TAM i.p.
7w
B
control
cKO
DKO
TKO
TH/NCL/DAPI
C
control
TKO
P53/TH
D
control
DKO
cKO
TKO
E
TH immunoraectivity (%)
160
140
120
100
80
60
40
20
0
*
**
F
Dopamine (ng/mg ww)
30
25
20
15
10
5
0
*
**
***
control
DKO
cKO
TKO

**Figure 6: Loss of DJ-1 and PINK1 does not exacerbate the toxic effects of nucleolar stress in DA neurons. A:** Experimental design scheme. **B:** Representative confocal images showing nucleolar integrity in DA neurons by immunofluorescent staining with NCL (red) and TH (green) antibodies in control, DJ-1/PINK1 double knock-out (DKO), TIF-IA conditional mutants (cKO) and TKO mice. **C:** Representative IHC images of p53 protein (brown) in TH positive neurons (blue) in control and TKO mice 7 weeks after TAM injections. Neurons showing increased p53 levels are indicated by arrowheads. **D**: Representative images of striatal TH immunoreactivity on vibratome sections of control, DJ-1/PINK1 double knock-out (DKO), TIF-IA conditional mutants (cKO) and TKO mice. **E:** Quantification of TH immunoreactivity in the striata of control (N=5), DKO (N=3), cKO (N=4) and TKO (N=5) mice. **F:** Analysis of dopamine content by HPLC-ED in the striata of control (N=13), DKO (N=9), cKO (N=4) and TKO (N=5) mice. Data are mean ± SEM; *, $p<0.05$; **, $p<0.01$; ***, $p<0.001$ as determined by one-way ANOVA followed by Tukey's multiple comparison test; ww: wet weight. Scale bar: B, 30 µm; C, 50 µm; D, 200µm.

**Tables**

**Table 1: Summary of the link between PD, PD-associated genes and rRNA synthesis based on present and previous work.**

| | **Sporadic PD** | **hA53T-SNCA/ PINK1 KO** | **PINK1 KO** | **DJ1/ PINK1 DKO** | **DJ-1 L166P** | **PARKIN cKO** |
|---|---|---|---|---|---|---|
| **TIF-IA** | - | - | = | = | nd | nd |
| **NPM** | - (Garcia-Esparcia et al., 2015) | = | = | = | nd | nd |
| **NCL** | - (Caudle et al., 2009) | = | = | = | nd | nd |
| **Pre-rRNA** | - (Kang and Shin, 2014) | - | = | = | + (Vilotti et al., 2012) | - (Kang and Shin, 2014) |

"-": reduced, "=": no change, "+": increased, nd: not determined

**Supplementary information**

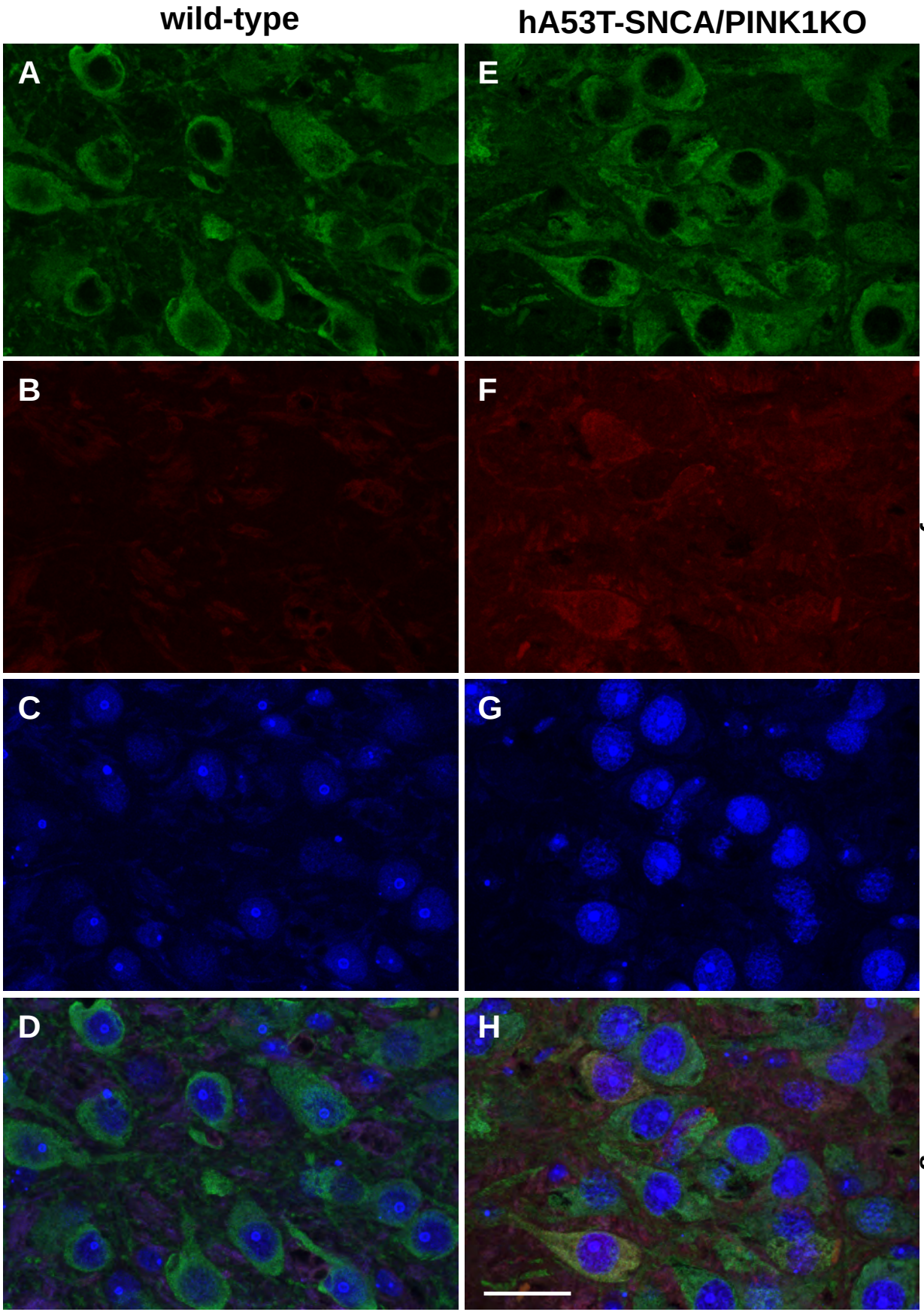


**Suppl. Fig. 1**

**Suppl. Figure 1**

**hA53T-SNCA is expressed in DA neurons in the cytoplasm and in the nucleolus.** Representative confocal microscopy images of paraffin sections immunostained with TH (green), human alpha-synuclein (red) and NCL (blue) specific antibodies from 3 month-old wild-type (**A-D**) and hA53T-SNCA overexpressing transgenic mice in a PINK1 KO background (hA53T-SNCA/PINK1KO) (**E-H**). Scale bar: 25 μm.

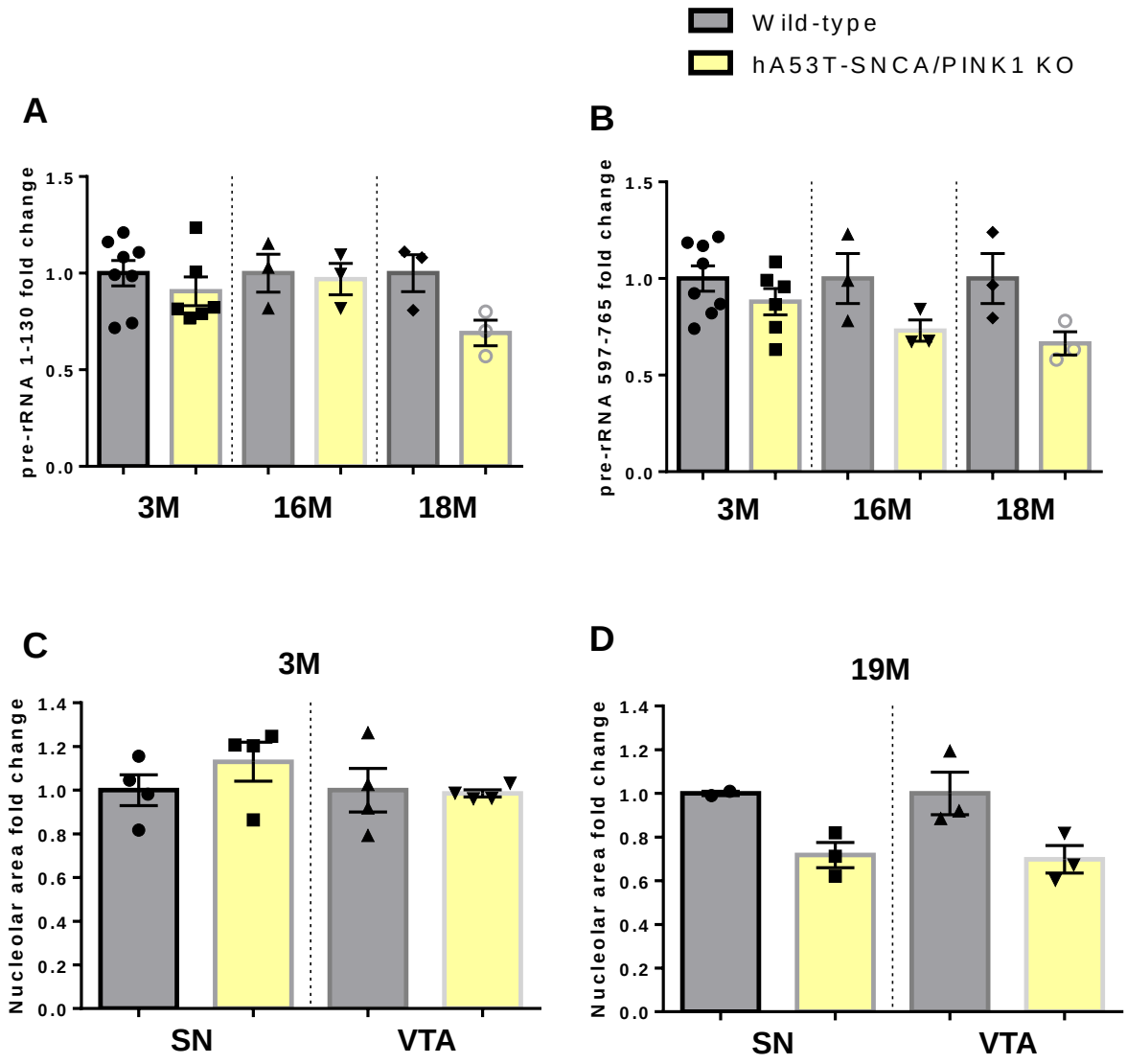


**Suppl. Fig. 2**

**Suppl. Figure 2: Individual data plots from Figure 2**

**A, B:** Analysis of pre-rRNA (1-130) and pre-rRNA (597-765) by qRT-PCR at 3, 16 and 18 months in the ventral midbrain of wild-type (N=8,3,3) and hA53T-SNCA/PINK1KO mice (N=6,3,3) expressed as fold change to respective controls and normalized by GAPDH. **C, D:** Quantification of the area occupied by the 47S staining in hA53T-SNCA/PINK1KO expressed as fold change relative to respective controls in SN and VTA at 3 and 19 months (N=4 and 3). Data are mean ± SEM.

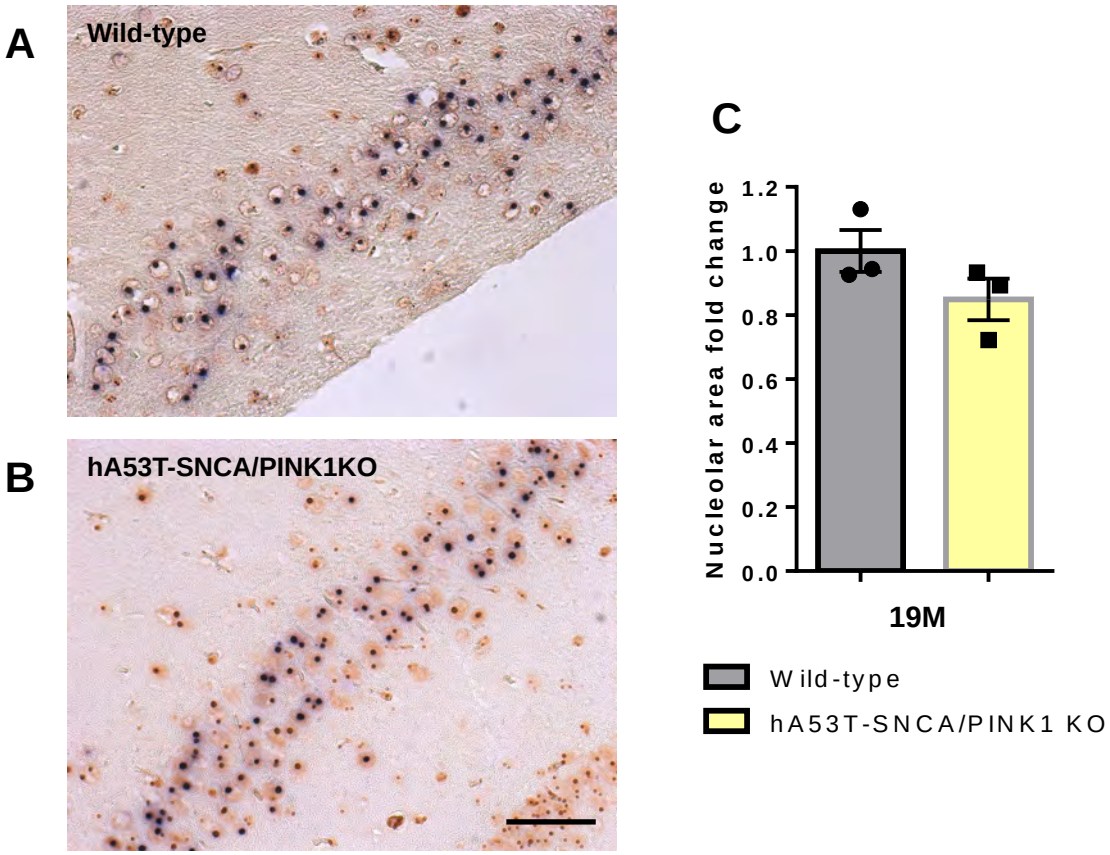


**Suppl. Fig. 3**

**Suppl. Figure 3: 47S pre-rRNA localization and nucleolar area in hippocampal neurons of hA53T-SNCA/PINK1KO mice.**

**A, B:** Representative images of ISH with 47S specific riboprobe (blue) and counterstained with Nuclear Fast Red at 19 months in CA1 of wild-type and hA53T-SNCA/PINK1KO mice. **C:** Quantification of the area occupied by the 47S staining in hA53T-SNCA/PINK1KO expressed as fold change relative to wild-type control at 19 months (N=3). Data are mean ± SEM.

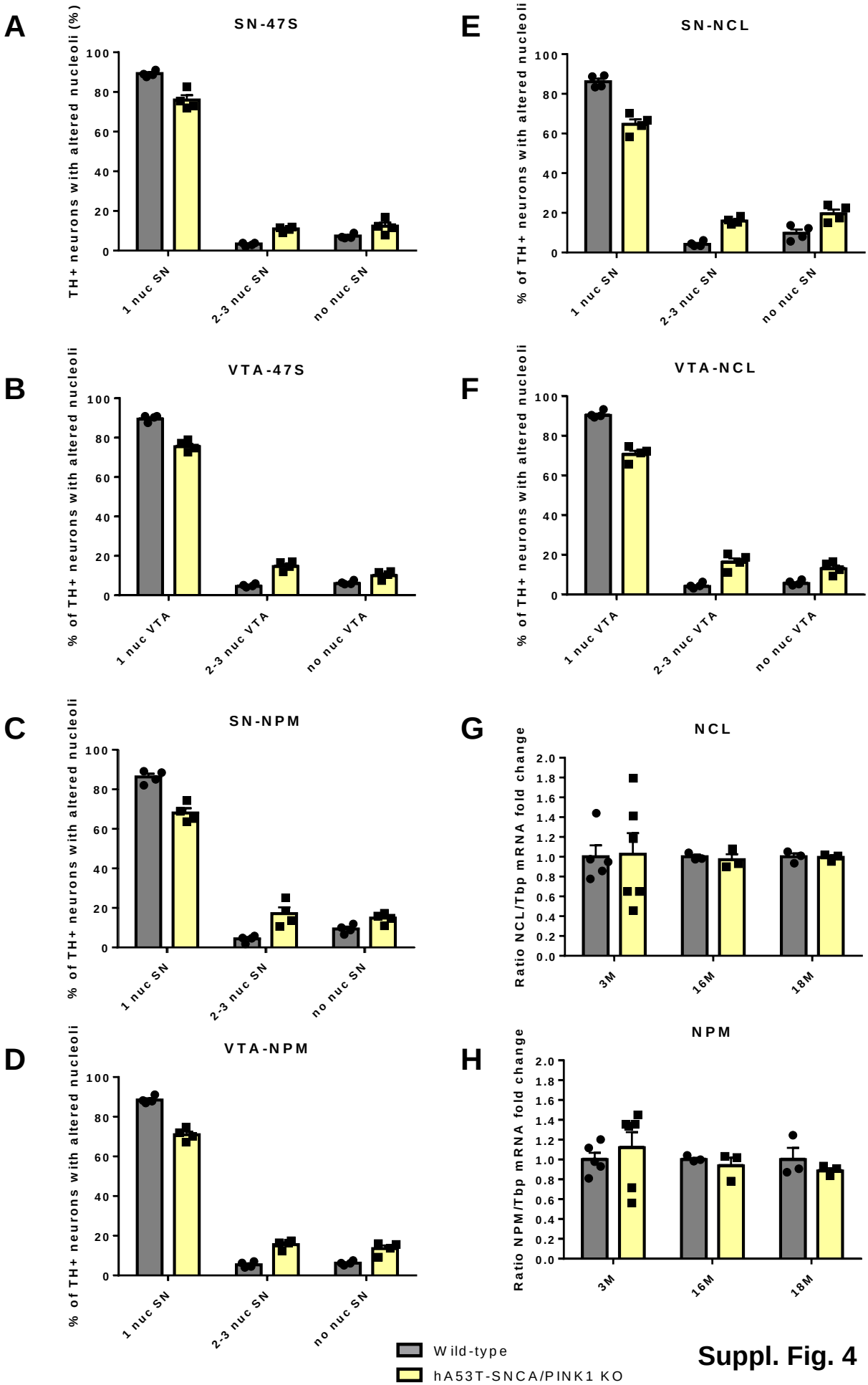
A
SN-47S
TH+ neurons with altered nucleoli (%)
1 nuc SN
2-3 nuc SN
no nuc SN
B
VTA-47S
% of TH+ neurons with altered nucleoli
1 nuc VTA
2-3 nuc VTA
no nuc VTA
C
SN-NPM
D
VTA-NPM
E
SN-NCL
F
VTA-NCL
G
NCL
Ratio NCL/Tbp mRNA fold change
3M
16M
18M
H
NPM
Ratio NPM/Tbp mRNA fold change
Wild-type
hA53T-SNCA/PINK1 KO

**Suppl. Fig. 4**

**Suppl. Figure 4: Individual data plots from Figure 3**

**A, B:** Quantification of the number of nucleoli detected by ISH with 47S specific riboprobe in TH positive neurons of 3 months old wild-type and hA53T-SNCA/PINK1KO mice (N=4) in SN (left) and VTA (right) expressed as percentage of TH positive neurons with 1, 2-3 or no nucleoli. Quantification of the number of nucleoli detected by NPM (**C, D**) and NCL (**E, F**) immunostaining in TH positive neurons of wild-type and hA53T-SNCA/PINK1KO mice (N=4) in SN and VTA expressed as percent of TH positive neurons with 1, 2-3 or no nucleoli. **G, H:** Analysis of NCL and NPM mRNA levels by qRT-PCR at 3, 16 and 18 months in wild type (N=5,3,3) and hA53T-SNCA/PINK1 KO mice (N=6,3,3) expressed as fold change to respective controls and normalized by Tbp. All data are mean ± SEM; nuc: nucleolus.

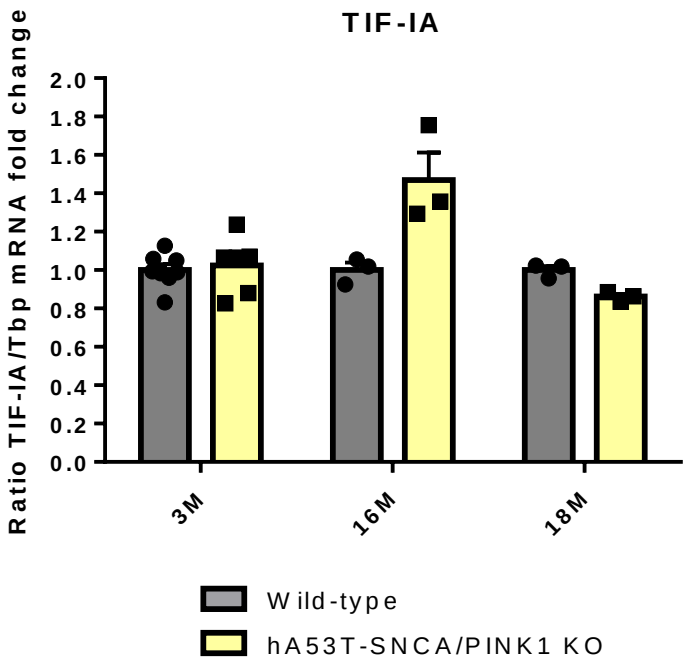


**Suppl. Fig. 5**

**Suppl. Figure 5: Individual data plot from Figure 4**

Analysis of TIF-IA expression by qRT-PCR in 3, 16 and 18 months old wild-type (N=8,3,3) and hA53T-SNCA/PINK1KO mice (N=6,3,3) expressed as fold change to respective controls normalized by Tbp. Data are mean ± SEM.

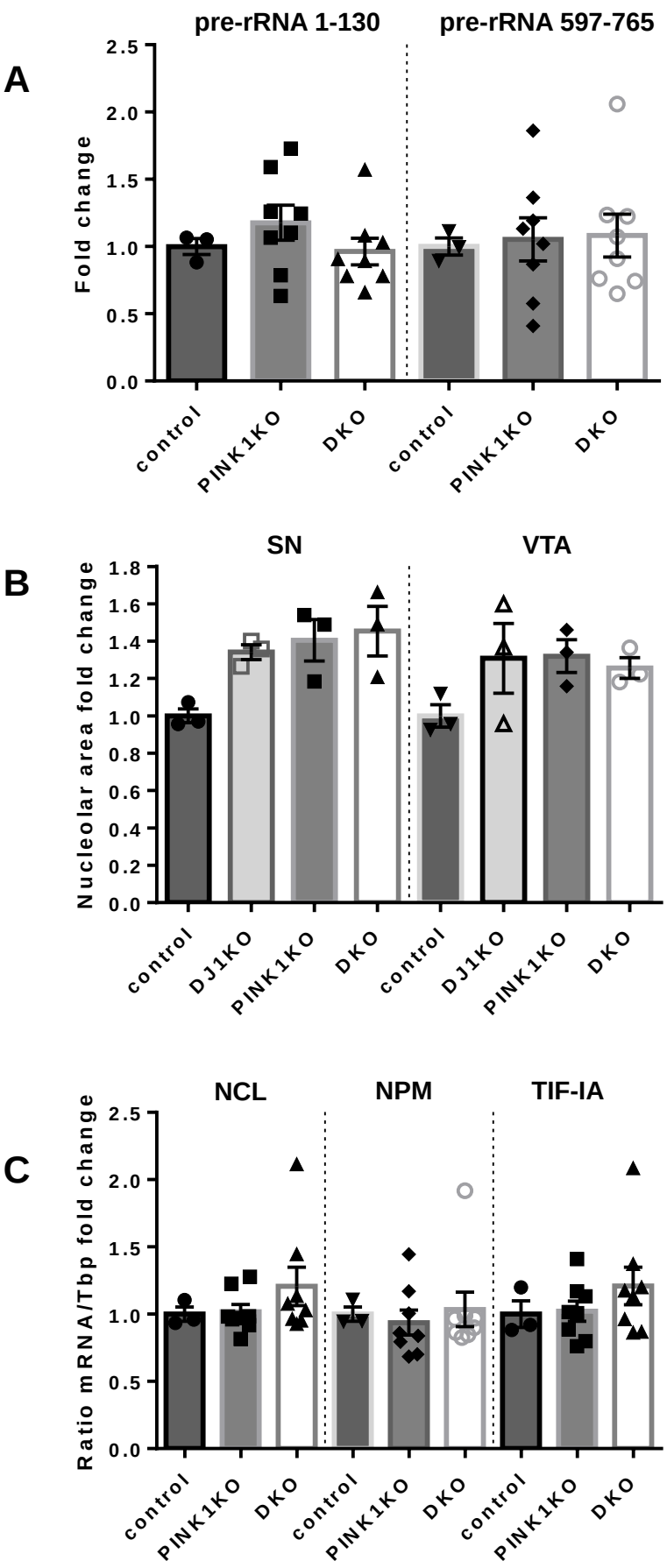


**Suppl. Fig. 6**

**Suppl. Figure 6: Individual data plots from Figure 5 including nucleolar area analysis for DJ-1 KO mice.**

**A:** Analysis of pre-rRNA (1-130) and pre-rRNA (597-765) by qRT-PCR in controls (N=3), PINK1 KO (N=8) and DJ-1/PINK1 DKO mice (N=8) expressed as fold change to respective controls normalized by GAPDH. **B:** Quantification of the area occupied by the 47S staining in control, DJ-1 KO, PINK1 KO and DKO mice (N=3) expressed as fold change relative to respective controls in SN and VTA. **C:** Analysis of NCL, NPM and TIF-IA mRNA levels by qRT-PCR in wild-type (N=3), PINK1 KO (N=8) and DJ-1/PINK1 DKO (N=8) mice at 9 months expressed as fold change to respective controls normalized by Tbp. All data are mean ± SEM.

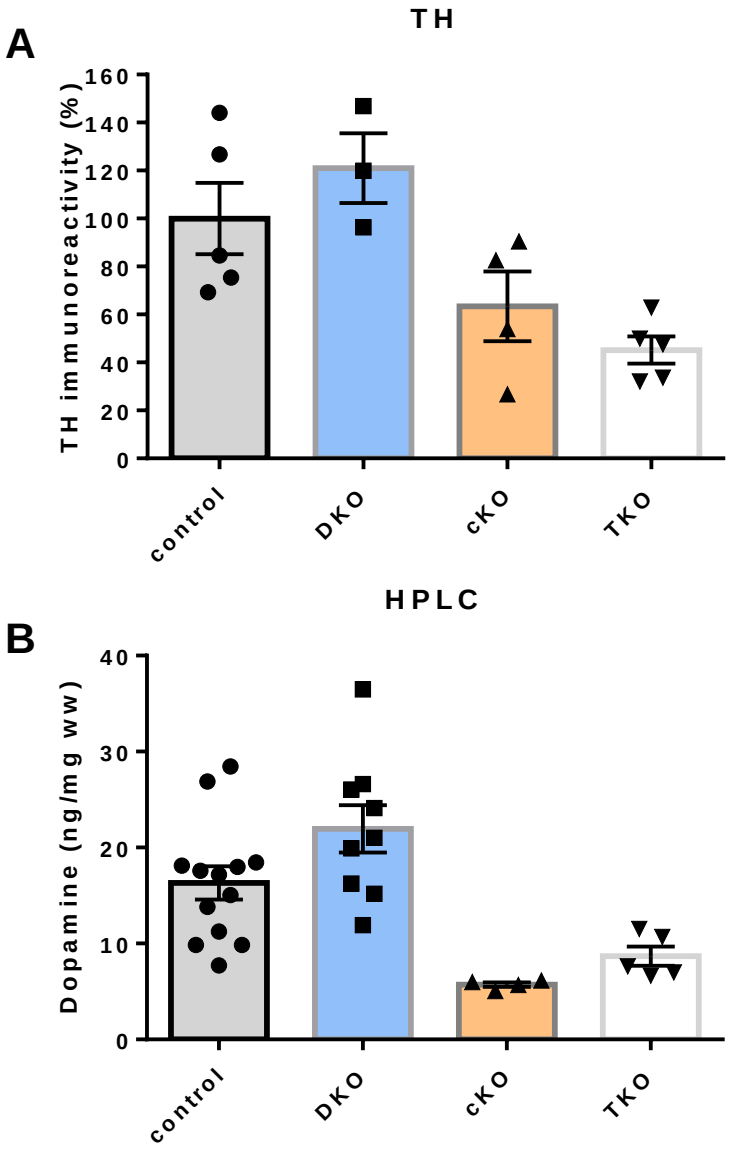


**Suppl. Fig. 7**

**Suppl. Figure 7: Individual data plots from Figure 6**

**A:** Quantification of TH immunoreactivity in the striata of control (N=5), DKO (N=3), cKO (N=4) and TKO (N=5) mice. **B:** Analysis of dopamine content by HPLC-ED in the striata of control (N=13), DKO (N=9), cKO (N=4) and TKO (N=5) mice. Data are mean ± SEM; ww: wet weight.